Computational modeling of stably stratified, turbulent shear flows

Hannibal Eie Fossum

Thesis submitted for the degree of Ph.D.

Department of Mathematics

© Hannibal Eie Fossum, 2015

Series of dissertations submitted to the
Faculty of Mathematics and Natural Sciences, University of Oslo
No. 1688

ISSN 1501-7710

All rights reserved. No part of this publication may be
reproduced or transmitted, in any form or by any means, without permission.

Cover: Hanne Baadsgaard Utigard.
Print production: John Grieg AS, Bergen.

Produced in co-operation with Akademika Publishing.
The thesis is produced by Akademika Publishing merely in connection with the thesis defence. Kindly direct all inquiries regarding the thesis to the copyright holder or the unit which grants the doctorate.

Abstract

The present thesis is motivated by the desire to understand and to predict the effects of stable stratification on turbulent flow and passive scalar dispersion.

A methodology which enables the simulation of stably stratified, turbulent boundary-layer flows in a flexible solver has been established. Data from highly resolved large-eddy simulations of channel flow and direct numerical simulation of free turbulent shear flow, originating from Kelvin-Helmholtz instabilities, is used to investigate the effects of stable stratification on turbulent shear flow and scalar dispersion. Changes in turbulence dynamics and structures have been of particular interest, as these areas are largely unexplored in the existing literature.

The present work suggests that, in channel flow, three distinct regions of the channel can be identified; the shear region closest to the wall, the transition region, and the buoyancy region in the center of the channel.

It has been established that the most obvious effects of imposed stable stratification are reduced vertical turbulent fluctuations and transport, as well as a related increase in turbulence anisotropy. Furthermore, the results reveal important changes in the structural state of the turbulence. The "compression" of vertical structures can be quantified by the structure dimensionality tensor, and this effect is demonstrated to be significant in some cases. The transition region in channel flow is strongly homogenized by increased stratification, which suggests an increased decoupling between the inner shear region and outer buoyancy region.

From the free-shear flow data, it appears that the Reynolds stress anisotropy increase up to a certain level of stratification, corresponding to a gradient Richardson number of approximately 0.4. For stronger stratification, however, the turbulence anisotropy is reduced, most likely caused by relaminarization. Moreover, analysis of the free-shear turbulence dynamics suggests that the shear production term *removes* energy from the turbulent field near the edge of the shear layer, whereas the buoyancy destruction term is an instigator of turbulence. It is shown that this is related to the observed turbulent flux reversal, i.e. a change in sign of turbulent shear stress, $\langle uw \rangle$. It is also found that, for the Reynolds numbers considered presently, the viscous dissipation rate is highly anisotropic.

Another interesting feature of free-shear flow is how the imposition of strong stable stratification seems to mimic the non-local pressure effects encountered in the vicinity of impenetrable walls. However, the kinematic blocking effect of walls does not seem to be emulated by the imposed stable stratification, despite the overall reduction of vertical velocity fluctuations. Turbulence models employed in stably stratified flows ought to include non-local information to incorporate important effects of stratification.

Due to changes in the turbulence field, passive scalar transport is altered significantly by stable stratification. In channel flow, the effect of stratification is stronger on scalar releases in the buoyancy region. Vertical scalar flux is reduced, leading to inhibited vertical dispersion and higher peak concentrations downstream than in the neutral case. For example, four boundary-layer lengths downstream, peak concentration was more than 50 % higher for $\mathrm{Ri}_\tau = 240$ compared to neutral flow. Whereas peak mean concentration downstream decays exponentially in the neutral case, this is not the case under imposed stratification. As a predictive tool, eddy-diffusivity models for scalar transport therefore need to take stratification into account.

Preface

This thesis is submitted in partial fulfillment of the degree of *philosophiae doctor* (Ph.D.) at the University of Oslo. The work presented here has been carried out between August 2011 and June 2015, mainly at the Norwegian Defence Research Institute (FFI).

The present thesis consists of four papers (see below) and an introduction. The introduction motivates the work that has been done, presents an overview of the theory used in the analysis carried out in the papers, and relates the papers to each other.

In addition to the introduction, this thesis consists of the following four papers:

Paper I: Fossum, H. E., Wingstedt, E. M. M., and Pettersson Reif, B. A. A model for the viscous dissipation rate in stably stratified, sheared turbulence. *Geophysical Research Letters*, 40(14):3744–3749, 2013.

Paper II: Wingstedt, E. M. M., Fossum, H. E., and Pettersson Reif, B. A. Anisotropy and shear-layer edge dynamics of statistically unsteady, stratified, sheared turbulence. *Physics of Fluids*, 27(6):065106, 2015.

Paper III: Fossum, H. E. Numerical simulation of stably stratified channel flow. Part I: Characterization, dynamics, and scalar transport.

Submitted to *Physics of Fluids* for publication in 2015.

Paper IV: Fossum, H. E. and Pettersson Reif, B. A. Numerical simulation of stably stratified channel flow. Part II: Turbulence structures.

Submitted to *Physics of Fluids* for publication in 2015.

Related work not included in the thesis: Fossum, H. E., Petterson Reif, B. A., Tutkun, M., and Gjesdal, T. On the Use of Computational Fluid Dynamics to Investigate Aerosol Dispersion in an Industrial Environment: A Case Study. *Boundary-Layer Meteorology*, 144:21–40, 2012.

Acknowledgments

First and foremost, I wish to thank my main supervisor, Prof. Bjørn Anders Pettersson Reif. He has provided invaluable guidance and motivation during my entire PhD period, and his level of insight and knowledge about turbulence still amazes me. In addition to our more academic discussions, we have also had several less mentally demanding conversations over a beer or two (or three) the past four years.

Furthermore, I am grateful to my other three supervisors, Prof. Øyvind Andreassen (the tensor guru), Dr. Erland Ørbekk (an actual rocket scientist!), and Prof. Atle Jensen ("Mr. Maritime Mechanics"). Vegard Sande at Nammo AS deserves special thanks as well, particularly for spending much time on administration and complicated forms on my behalf, all the while remaining positive.

I am fortunate to have a lot of good friends and colleagues both at the University of Oslo (UiO) and at the Norwegian Defence Research Establishment (FFI). I am particularly grateful to my co-author, Emma Wingstedt, and my "office-mate", Magnus Vartdal, for endless discussions about fluid mechanics, turbulence, and stratification, as well as traffic regulations, social norms, politics, the superiority of Norway (or was it Sweden?), and beer.

Espen (ESPN, selv Espen, Espa) has also provided me with valuable questions and discussions about turbulence, as well as many ridiculous conversations (in a good way). Andreas, Daniel, Marianne (when she isn't "coming later"), Pål-Martin, Carina, Tor-Erik (el Torro) and Maria have made sure the lunches have been enjoyable. The "veterans" on the second floor, Carl-Erik, Thor, and Anders H., have provided useful inputs on numerics and visualization as well as interesting conversations about orienteering, renovation, neighborhood conflicts, and kids.

A special thank-you is reserved for two of my earlier teachers: Gunnar Henriksen was the first to show me that math could actually be fun, logical and quite easy! Without him, I might have ended up as a lawyer – or even worse... Sven-Erik Topp then helped me realize that math really wasn't *that* easy, and that I actually had to do the work as well – the seemingly endless list of calculus problems he supplied was what enabled me to use math as an efficient tool when I needed it. (Without this necessary lesson, I probably never would have dared to open a book on fluid mechanics.)

Finally, I am very grateful for the support of my family. My parents, Elin and Tor Hannibal, and my in-laws, Bente and Per (and grandmother-in-law, Berit), have cheered me on with unwavering belief in me (even if they've needed to ask me several times what I'm actually researching). My wonderful wife and great love, Camilla, has never doubted my ability to finish this thesis, even when I've doubted myself, and she has tried really hard to understand this weird stuff I'm doing. (However, I think her idea of the computer cluster as a social meeting point at work lost its charm once she realized that no one ever had to actually go to the cluster physically to use it.) Thank you, Camilla!

Contents

Chapter 1

Background

The world around us is filled with fluids!

Water, oil, milk, honey, and blood are all examples of liquids that can be seen and touched. The air that surrounds us cannot be seen, but its effects are visible as leaves blowing in the wind, smoke spreading from a chimney, or waves on the sea surface. You can feel the air when the wind blows, and you respond to pressure fluctuations when someone speaks to you.

How can such vast and complex fluid motions as winds, waves, or currents be described, let alone predicted? Often, one begins by simplifying it, or by looking at only some parts of the system separately.

The present thesis is motivated by the desire to understand the interaction between *turbulence* and *stable stratification*. This is an important aspect of many complex fluid flows around us, most notably atmospheric flows, as shown in Figure 1.1. A deeper understanding of the stratification-turbulence interaction can improve the ability to model and predict such flows, subsequently allowing improvements in weather forecasting and the design of industrial machinery.

Turbulence constitutes the chaotic system of whirls and eddies that is present in virtually all real-life flows; it is the reason why smoke plumes always seem to have complex structures of varying size, and why airplanes occasionally start shaking during flight. Stable stratification, sometimes also referred to as inversion, occurs when the density of a fluid decreases with altitude, such as in oceans due to different salinity levels and in the atmosphere because of temperature variations.

The atmospheric boundary layer (ABL) of our planet is a large part of the

Figure 1.1: Fog, "captured" by stable stratification, envelopes Vancouver, Canada. Photo courtesy of Michael Wheatley, *Encyclopædia Britannica ImageQuest*.

global weather system; it is the 1–2 km deep layer of air which is affected by the Earth's surface, and the local weather we experience at the surface is a direct consequence of the turbulent motions in the ABL. Dispersion of pollutants or other contaminants is an important example of processes in the ABL that are significantly affected by turbulence and, if present, stable stratification.

Transport and dispersion of any passive contaminant are governed by turbulence and mean flow advection, rather than by molecular diffusion; the contaminant simply follows the large-scale three-dimensional and time-dependent velocity field. Passive contaminant transport is therefore expected to respond significantly to changes in the kinematic structure of the flow field caused by the imposition of a stably stratified background.

As an example, a dangerous pollutant released from an industrial chimney might diffuse quickly to become sufficiently diluted and thus relatively safe on a warm summer day. However, at night or in the winter, when the Earth's surface is cold and the air becomes stably stratified, the turbulence levels will decrease. This can lead to significantly reduced vertical dispersion of the pollutant, in turn

causing the pollutant to remain concentrated and dangerous for far longer.

Many features of stably stratified fluid flows are challenging to predict and to model mathematically. The practical importance of stably stratified shear turbulence in general and its relevance to contaminant transport and dispersion in particular constitute the primary motivations for the present study.

Whereas previous studies, both experimental and numerical, have revealed many aspects of how stable stratification affects turbulent motion, the dynamics and structure of the turbulence have not received the same attention. The present thesis seeks to shed more light on these features of stably stratified, turbulent shear flows by means of high-fidelity numerical simulations.

1.1 Thesis objectives

The main objectives of the thesis can be summarized as follows.

- Establish a methodology which enables the simulation of stably stratified, turbulent boundary-layer flows in a flexible solver which can easily be extended to more complex problems.
- Investigate how the imposition of stable stratification affects turbulent shear flow, with particular emphasis on the turbulence dynamics and structures.
- Examine the effects of stable stratification on scalar dispersion in a turbulent boundary layer.

The main conclusions of the present thesis are summarized in Section 7.

1.2 Thesis outline

The remainder of this introduction is written with the goal of combining a coherent organization of theory with a sense of motivation behind the thesis as a whole.

Firstly, some background on the subject of turbulence is presented in Section 2; definitions, notation, governing equations, and tools to quantify and analyze turbulent flows will be presented. This section forms the basis for most of the analysis carried out in Papers II–IV.

Section 3 defines the concepts and theory necessary to understand and describe stably stratified, turbulent flow, with particular emphasis on the Boussinesq approximation. The ideas of this section underlie the mathematical modeling of stratification in the simulations described in Papers I–IV.

In Section 4, the attention is then turned toward the ABL. While this is not a research topic of this thesis, it is relevant as context. Additionally, the section contains a subsection on internal gravity waves, an ABL phenomenon which forms the "physical" foundation of the simulations in Papers I and II.

Fully-developed channel flow constitutes one of the most basic non-homogeneous turbulent shear flows, and it serves as a first approximation to the ABL. Section 5 summarizes the most relevant theory and literature on this subject, which forms the basis of the simulations in Papers III and IV.

The numerical solution of complex fluid flow problems would not be possible without computational resources. In Section 6, the Computational Fluid Dynamics (CFD) methodology is presented, focusing especially on the finite-volume method (FVM) that underlies the simulations in Papers III and IV.

Finally, the most important conclusions of this thesis, as well as the conclusions of each individual paper, are summarized in Section 7.

Chapter 2

The mystery of turbulence

> Turbulence is the most important unsolved problem of classical physics.
>
> – *Richard P. Feynman* (Feynman et al., 1963)

The physics of turbulent flows represent a considerable and important scientific challenge. Turbulence is present in virtually all naturally occurring flows of gases and liquids, and it is a highly relevant problem to engineers as well as physicists. Turbulence affects flows around moving objects such as airplanes, cars, and ships, it has a significant impact on pipe flows, such as oil and gas transport, ventilation systems, or the flow inside the human airways, and it is a major part of any meteorological system, both globally and locally. Physical and chemical processes occurring in for example combustion engines or industrial production are highly dependent on turbulent mixing.

As a laminar flow undergoes transition to turbulence, illustrated by the buoyancy-driven smoke plume in Figure 2.1, important aspects of the flow change. Mixing processes become significantly more efficient due to turbulent transport (also referred to as turbulent diffusion). It can be shown from an order-of-magnitude analysis that turbulent mixing in air is usually thousands of times more effective than molecular diffusion!

In wall-bounded flows, the thickness of the boundary layer increases as the flow develops downstream, and the mean velocity profile changes. In particular,

Figure 2.1: Warm smoke rising in surrounding air, visualizing the transition from laminar to turbulent flow. Photo courtesy of Jan Olav Langseth, *Norwegian Defence Research Establishment*.

the velocity gradient close to the wall increases, causing increased wall friction. This in turn means that a much larger pressure gradient is required for a turbulent flow to maintain the same volume flow as a laminar flow. Turbulent mixing of momentum thus increases the pressure loss in wall-bounded flows.

The equations governing fluid flows are well-known, but in most cases they are difficult to solve exactly. For turbulent flows in general, the equations cannot be solved exactly at all. Despite the increase in computing power over the last three decades, as well as the emergence of numerous turbulence models, the *nature* of turbulence remains elusive, as does the ability to make good predictions for many turbulent flows.

Even the definition of a turbulent flow is incomplete at best: A turbulent flow contains a large range of temporal and spatial scales. It must be four-dimensional (three spatial dimensions as well as time) and cannot be irrotational. Its visual structure appears chaotic, with eddies of varying sizes present simultaneously, yet it also contains recognizable patterns, visible e.g. in Figure 2.1. Fundamentally

deterministic in nature, turbulent flows are random and stochastic[1] in practice.

A more detailed list of requirements for turbulence is provided in the classic textbook by Tennekes and Lumley (1972, p. 1).

Mathematically, the difficulty of predicting turbulent flows arises from the nonlinear term in the conservation equation for momentum. A variety of turbulence models have emerged to address this problem, a topic which will be discussed in more detail shortly.

Osborne Reynolds popularized the so-called Reynolds number in 1883 during his work on pipe flow (Reynolds, 1883). He realized that the dimensionless ratio $\mathrm{Re} = UL/\nu$ was the relevant non-dimensional parameter to describe the onset of turbulence in the pipe. Here, U and L are characteristic velocity and length scales, respectively, and ν is the kinematic viscosity of the fluid. In a subsequent paper (Reynolds, 1894), he quotes the critical Reynolds number range as 1,900 $< \mathrm{Re} <$ 2,000. This approximate value is still generally valid, but it has been demonstrated that the upper and lower bounds can vary significantly in practice. The Reynolds number represents a ratio of inertial to viscous forces in the fluid, and a range of different kinds of Reynolds numbers exists, depending on which length and velocity scales that are used in calculating the number.

Two important subclasses of turbulent flows are *isotropic* turbulence and *homogeneous* turbulence. The latter is a state of statistically identical turbulence at all spatial locations (but with possible temporal variations). This means that all correlations of fluctuating fields are the same at every position. Examples include certain cases of parallel shear flow, channel flows (homogeneous in two directions) and grid-generated turbulence. The latter is also a case of isotropic turbulence, in which the turbulence characteristics (such as turbulent stresses) are the same in all directions. This implies turbulence which is invariant to rotation, translation and reflection of the coordinate system. It can be shown that isotropic turbulence is always homogeneous.

Turbulent flows exhibit a wide range of scales. Generally, "more turbulence" – i.e. a higher Reynolds number – is associated with a larger separation between the largest and smallest spatial and temporal scales. Larger scale separations also entail more demanding computational-grid requirements; to resolve all turbulent scales, the domain must be large enough to contain the largest scales of motions

[1] Here, the notation of Wyngaard (2010) is adopted, see Section 2.2 for details.

while being sufficiently resolved to capture the smallest scales. The number of grid cells required to fully resolve a turbulent flow scales as $N_{\text{cells}} \sim \text{Re}^{9/4}$. Given that the bulk Reynolds number for e.g. atmospheric flows might be $\mathcal{O}(10^6)$ or several orders of magnitude larger, this puts severe limitations on the ability to predict turbulent flows exactly. The use of turbulence models aims to reduce the computational requirements associated with numerical fluid flow simulations.

The largest scales of turbulence, sometimes referred to as the *integral scales*, are related to the distance over which a turbulent flow field, e.g. velocity, is correlated with itself. Roughly, the integral scales are usually on the same order of magnitude as the geometry of the problem, such as the pipe diameter in pipe flow, or the boundary layer depth in wind field simulations. Most of the turbulence kinetic energy in a turbulent flow is contained in the large-scale motions.

The smallest scales of turbulence are referred to as the Kolmogorov microscales. Below these scales, the fluid viscosity has transformed all the kinetic energy of the turbulent motions into thermal energy in a process called *viscous dissipation* or *turbulent dissipation*. Kolmogorov (1941b) hypothesized that these small scales only depend on the fluid viscosity and the dissipation rate, thus enabling the use of dimensional analysis to find expressions for the small spatial, temporal, and velocity scales.

Kolmogorov also assumed that the smallest turbulence scales can be approximated to be isotropic, and hence universal, for all turbulent flows at a sufficiently high Reynolds number, i.e. that the smaller scales were independent of large-scale flow features. The latter, in contrast, are dictated by large-scale features such as the geometry of the flow domain and mean shear. Flows that are isotropic only on the small scales are said to be *locally isotropic*. Recently, it has been shown that the local isotropy hypothesis is not generally valid (except perhaps in the limit of infinite Reynolds number) (Wyngaard, 2010, p. 320).

2.1 Governing equations of fluid motion

The governing equations of fluid motion state that mass and momentum are conserved and are thus referred to as conservation equations. The conservation equation for momentum follows from Newton's second law.

Through the entire thesis, a Newtonian, incompressible fluid is considered. The former specification implies a linear relationship between stress and strain in the fluid, whereas the incompressibility constraint enforces constant density everywhere in the fluid. An important consequence of the incompressibility approximation is the instantaneous transport of pressure fluctuations (such as sound waves). Everyday fluid flows usually behave in a Newtonian and incompressible manner. Notable exceptions include fluid flow approaching the speed of sound (e.g. transonic flight), shock waves (e.g. detonations), or flows of viscoelastic fluids (e.g. various pastes).

Throughout this introduction, as well as the papers included in the thesis, index notation is used in conjunction with Einstein's summation convention. Unless stated otherwise, free indices range from 1 to 3, and repeated indices imply summation.

A Cartesian coordinate system is assumed. The general spatial position vector is given by

$$\boldsymbol{x} = (x_1, x_2, x_3) = (x, y, z),$$

whereas time is denoted t. In the present thesis, x will generally be taken as the streamwise direction, y is the spanwise direction, and z is the vertical or wall-normal direction. The corresponding three-dimensional instantaneous velocity vector field is denoted

$$\begin{aligned}\tilde{\boldsymbol{u}}(\boldsymbol{x}, t) &= (\tilde{u}_1(\boldsymbol{x}, t), \tilde{u}_2(\boldsymbol{x}, t), \tilde{u}_3(\boldsymbol{x}, t)) \\ &= (\tilde{u}(\boldsymbol{x}, t), \tilde{v}(\boldsymbol{x}, t), \tilde{w}(\boldsymbol{x}, t)),\end{aligned}$$

and the three-dimensional instantaneous pressure field is denoted $\tilde{p}(\boldsymbol{x}, t)$. Moreover, partial differentiation is abbreviated by

$$\begin{aligned}\partial_i &= \partial/\partial x_i = (\partial/\partial x, \partial/\partial y, \partial/\partial z), \\ \partial_t &= \partial/\partial t,\end{aligned}$$

for spatial and temporal gradients, respectively, when this is beneficial.

The conservation equations for momentum and mass for an incompressible,

Newtonian fluid can be written

$$\partial_t \tilde{u}_i + \tilde{u}_k \partial_k \tilde{u}_i = -\frac{1}{\rho}\partial_i \tilde{p} + \nu \partial_k \partial_k \tilde{u}_i + F_{V,i}, \tag{2.1}$$

$$\partial_k \tilde{u}_k = 0, \tag{2.2}$$

respectively. Here, ρ is the (constant) fluid density and $\nu = \mu/\rho$ is the kinematic viscosity, with μ being the dynamic viscosity. The term $F_{V,i}$ represents any other volume forces affecting the fluid, such as buoyancy or rotation.

If scalars, such as gases, aerosols, or temperature, are transported in the fluid, each of them is also governed by its own transport equation, reading

$$\partial_t \tilde{c} + u_k \partial_k \tilde{c} = \gamma \partial_k \partial_k \tilde{c}, \tag{2.3}$$

in which $\tilde{c} = \tilde{c}(\boldsymbol{x}, t)$ is the transported scalar, and γ is its diffusivity.

Generally, for the system of partial differential equations to have a unique solution, initial and boundary conditions must be provided. In a few simplified cases, such as steady-state laminar pipe flow, only boundary conditions are required, and the equations can even be solved analytically. In more complex cases, numerical algorithms must be employed to obtain three-dimensional, time-dependent solutions.

The second term on the left-hand side of Eq. (2.1) is the advective term. Its nonlinearity is what makes the solution of this equation system so susceptible to minimal perturbations in initial and boundary conditions, which in turn may lead to the turbulent nature of the solution. The nonlinearity generally makes the equations impossible to solve analytically and even with the help of powerful computers. Only a narrow range of real-life problems can be solved exactly, by so-called direct numerical simulation (DNS). For instance, neither the flow around a full-scale aircraft in flight nor the local wind field of a small weather system can be predicted without resorting to approximate models related to this nonlinearity, so-called *turbulence models*.

Turbulence models generally fall into two main categories: Reynolds-averaged Navier-Stokes (RANS) models and large-eddy simulation (LES) models. Other models also exist, but these two categories are most common.

The simulation results utilized in Papers I and II are results of a DNS, whereas

those reported in Papers III and IV are based on LES data. The LES methodology used in the latter papers is discussed in detail in Section 2.5.

2.2 Statistical representation

A turbulent flow field is of random and stochastic nature. Here, the distinction of Wyngaard (2010, p. 15) is adopted; the random nature of a flow field implies that each flow realization is unique, whereas the irregular variations of the field fluctuations in time and space constitutes the stochastic character of a given realization.

The Reynolds decomposition separates a (four-dimensional) turbulent field into two parts: By averaging the field, the *mean flow field* is obtained, and the difference between the full field and the mean field then comprise the *fluctuating flow field*. Mathematically, the Reynolds decompositions can be written

$$\begin{aligned} \tilde{u}_i &= U_i + u_i, \\ \tilde{p} &= P + p, \\ \tilde{c} &= C + c \end{aligned}$$

for the velocity field, pressure field and an arbitrary scalar field, respectively. Here, symbols marked by a tilde ($\tilde{\cdot}$) denotes the full four-dimensional field, whereas the uppercase and lowercase symbols denote mean and fluctuating fields, respectively. Note that the average of a mean field returns the same mean field, whereas the average of a fluctuating field is identically zero.

Fundamentally, the averaging procedure is an ensemble average of infinitely many flow realizations, but in practice a finite spatial or temporal average is used (or a combination of both), e.g. for a temporal average of a statistically steady velocity field, $U_i(\boldsymbol{x}) = \langle \tilde{u}_i \rangle \approx \int_0^T U_i(\boldsymbol{x}, t)\,\mathrm{d}t$, in which $\langle \cdot \rangle$ denotes the averaging process, and T is the averaging period. Such an approximation to the true average is valid only if the flow is ergodic with respect to the averaging dimension (time t in the previous example), i.e. homogeneous in one or more spatial directions (for spatial averaging) or statistically steady (for temporal averaging).

By utilizing Reynolds decompositions in Eqs. (2.1) and (2.2) and then apply averaging, the RANS equations are obtained. These equations govern the evolution of the mean flow fields and form the basis for the RANS class of turbulence

models. The transport equation for a mean scalar field can be derived in a similar manner.

The RANS equations are very similar to Eqs. (2.1) and (2.2), with the exception of an additional source term, $\partial_j r_{ij}$, in which r_{ij} is referred to as the Reynolds stresses. This term originates from the advection term in Eq. (2.1). The Reynolds-stress tensor can be written

$$r_{ij} = \langle u_i u_j \rangle,$$

i.e. each tensor component is a single-point correlation between fluctuating velocity vector components. The Reynolds stress tensor does not really represent physical stresses, but it has the same units. Physically, it is associated with momentum transport due to turbulent fluctuations, so-called turbulent momentum flux.

By subtracting the RANS equations from Eqs. (2.1) and (2.2), equations governing fluctuating mass and momentum transport are obtained. From these, the *Reynolds stress transport equation* (RSTE) can be derived. The result is

$$\begin{aligned} \partial_t \langle u_i u_j \rangle + U_k \partial_k \langle u_i u_j \rangle = P_{ij} + \phi_{ij} - \varepsilon_{ij} - \big(\partial_i \langle u_j p \rangle + \partial_j \langle u_i p \rangle\big)/\rho \\ + \partial_k \big[\nu \partial_k \langle u_i u_j \rangle - \langle u_i u_j u_k \rangle, \big] \end{aligned} \tag{2.4}$$

where $P_{ij} = -\big[\langle u_i u_k \rangle \partial_k U_j + \langle u_j u_k \rangle \partial_k U_i\big]$ and $\varepsilon_{ij} = 2\nu \langle \partial_k u_i \partial_k u_j \rangle$ are the production and viscous dissipation rates of Reynolds stress, respectively, and $\phi_{ij} = \langle p(\partial_i u_j + \partial_j u_i) \rangle / \rho$ is the pressure-strain rate correlation. The last two terms on the first line of Eq. (2.4) represents pressure diffusion, and the terms on the bottom line are viscous diffusion and turbulent diffusion (turbulent transport), respectively.

The turbulence kinetic energy is defined by an index contraction on the Reynolds stresses, i.e. $k = \frac{1}{2}\langle u_i u_i \rangle$. Hence, along with the definition of k, index contraction on the RSTE yields the turbulence kinetic energy transport equation.

Both in experimental work and numerical simulations, the dissipation rate, ε_{ij}, in the RSTE often proves particularly cumbersome. It is essential to the turbulence kinetic energy cascade, but due to the local nature of the term (owing to the gradients of fluctuating fields in its definition), it is notoriously difficult both to measure and compute.

Dissipation occurs on the smallest scales of turbulence, and thus very sensit-

ive and microscopic experimental equipment is required to measure even a single component of the dissipation tensor. Similarly, finely resolved computational grids and accurate numerical algorithms are needed to correctly calculate the dissipation rate in a numerical simulation. Simulations in which a correctly computed dissipation rate tensor is important can generally be done only with DNS.

The isotropic formulation (see e.g., Thoroddsen and Van Atta, 1992, for derivation), where isotropic turbulence is assumed, is among the most used and well-known dissipation rate models used by experimentalists, requiring the measurement of only one (arbitrary) component of the fluctuating velocity gradient. The model is of the form

$$\varepsilon_{\mathrm{iso}} = C_{\varepsilon,\mathrm{iso}} \nu \langle (\partial_i u_j)^2 \rangle,$$

in which $C_{\varepsilon,\mathrm{iso}}$ takes one of two known values, depending on which velocity gradient is used.

In many real-life flows, such as geophysical flows affected by rotation and buoyancy, turbulence is not locally isotropic. In such flows, the isotropic model is a poor approximation of the true dissipation rate. In Paper I, an analytic method to derive an algebraic model for the dissipation rate of turbulence kinetic energy is presented. The method is based on first principles considering stratified, turbulent shear flow in the limit of local isotropy. A new model is derived, and it is demonstrated that it performs very well, particularly in cases where the background stratification becomes dynamically dominating.

2.3 Statistical description

To describe and quantify turbulence, a distinction can be made between global (or bulk) characteristics and pointwise measures. The former provides a classification of a specific turbulent flow as a whole, whereas the latter yields details about local flow conditions.

The bulk and friction Reynolds numbers are examples of global characteristics, as is the (global) friction factor. Other characterizations include bulk or centerline velocities, global pressure values, or maximum or average turbulence intensities.

The friction Reynolds number, $\mathrm{Re}_\tau = u_\tau L/\nu$ (cf. Section 5), is a measure of

the relative importance of inertial forces to viscous forces. Here, L is a characteristic length scale, such as boundary-layer thickness, pipe diameter, or building height, and u_τ is the friction velocity (cf. Section 5). Higher values of Re_τ implies "more turbulence", i.e. increased wall friction, and larger separation between large and small turbulent scales.

The Reynolds stresses represent turbulent momentum fluxes. Similarly, turbulent fluxes are associated with scalar flow fields, if such exist. In the case of a concentration field, $\tilde{c}$, the turbulent fluxes, $\langle u_i c \rangle$, quantifies the transport of concentration by turbulent motion.

The Reynolds-stress tensor generally contains six independent components. In order to reduce these data to a more compact form, the *invariants* of the tensor is sometimes considered. The general principle can be applied to any tensor, and the resulting invariants are independent of the global coordinate system.

By writing a second-order symmetric tensor, x_{ij}, in terms of its principal axes, only the diagonal components of the resulting tensor, i.e. the eigenvalues of x_{ij}, will be nonzero. Tensor eigenvalues are one example of tensor invariants.

Note that by reducing the six independent components of x_{ij} into three invariants, no information is necessarily lost: The principle axes, i.e. the eigenvectors of x_{ij} which emerge from the process of transforming x_{ij} into its eigenvector coordinate system, contain the remaining directional information.

For symmetric second-order tensors, another related set of tensor invariants can be obtained without calculating eigenvalues and eigenvectors explicitly:

$$I_x = x_{ii}, \tag{2.5}$$

$$II_x = -\frac{1}{2} x_{ij} x_{ji}, \tag{2.6}$$

$$III_x = \frac{1}{3} x_{ij} x_{jk} x_{ki}. \tag{2.7}$$

Here, I_x, II_x, and III_x are the first, second, and third invariants, respectively, of the second-order tensor x_{ij}. For trace-free tensors, only two of the three invariants are independent; the first invariant is simply $I_x = x_{ii} = 0$.

Usually, the trace-free, positive semi-definite Reynolds stress anisotropy tensor is calculated via

$$b_{ij} = \langle u_i u_j \rangle / \langle u_k u_k \rangle - \delta_{ij}/3,$$

and the invariants II_b and III_b of the anisotropy tensor are considered.

It follows from the definitions of the invariants that for trace-free, positive semi-definite tensors, $(II_{\min}, II_{\max}) = (-1/3, 0)$ and $(III_{\min}, III_{\max}) = (-1/108, 2/27)$. In the $(III, -II)$ state space, called the *anisotropy invariant map*, the points $(0, 0)$, $(2/27, 1/3)$, and $(-1/108, 1/12)$ define three vertices, as shown in Figure 2.2. These three vertices and the curves connecting them are commonly referred to as the *Lumley triangle* (Lumley and Newman, 1977), within which all possible states are located.

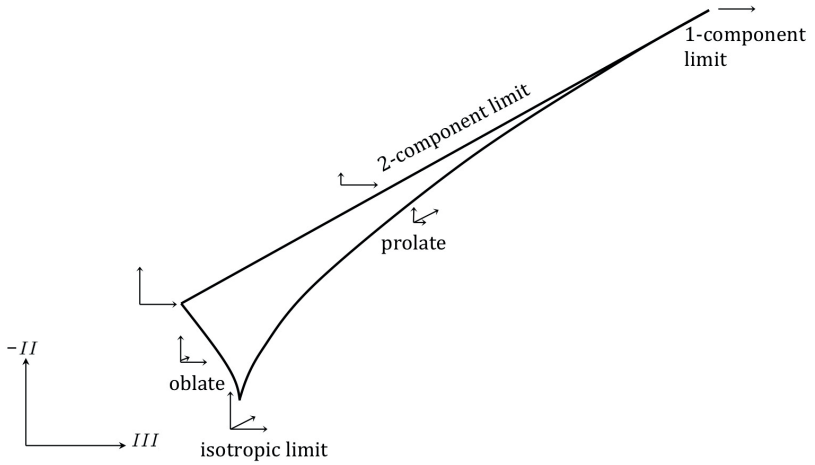

Figure 2.2: The Lumley triangle.

II_b measures the degree of anisotropy of the tensor; $II_b = 0$ represents an isotropic state, and larger negative values indicate increasing anisotropy levels. $III_b > 0$ indicates one dominating tensor component (prolate), whereas $III_b < 0$ implies two dominating components (oblate) (see Figure 2.2).

Turbulence is inherently a three-dimensional (and transient) phenomenon. Hence, important aspects of turbulent flows may be missing from single-point measures. To gain more insight into the spatiotemporal structure of turbulence, two-point correlations and energy spectra can be computed.

Two-point correlations are constructed from fluctuating flow fields at two locations separated by a vector $\boldsymbol{r} = (r_1, r_2, r_3)$, as illustrated in Figure 2.3. The most commonly used correlation involves only the velocity field, but pressure or scalar field correlations also exist, as well as two-point pressure-velocity correlations. The two-point velocity correlation is given by

$$R_{ij}(\boldsymbol{x}, \boldsymbol{r}) = \langle u_i(\boldsymbol{x}) u_j(\boldsymbol{x} + \boldsymbol{r}) \rangle. \tag{2.8}$$

By replacing $\boldsymbol{r}$ by the time coordinate, t, a temporal two-point correlation is obtained. In certain flow configurations, Taylor's "frozen turbulence" hypothesis is (approximately) valid, i.e. $\partial_t(\cdot) \simeq -U\partial_1(\cdot)$, and the temporal and streamwise spatial correlations are equivalent. Note that when $\boldsymbol{r} \to 0$, then $R_{ij} \to r_{ij}$, i.e. the two-point velocity correlation approaches the single-point Reynolds stress tensor.

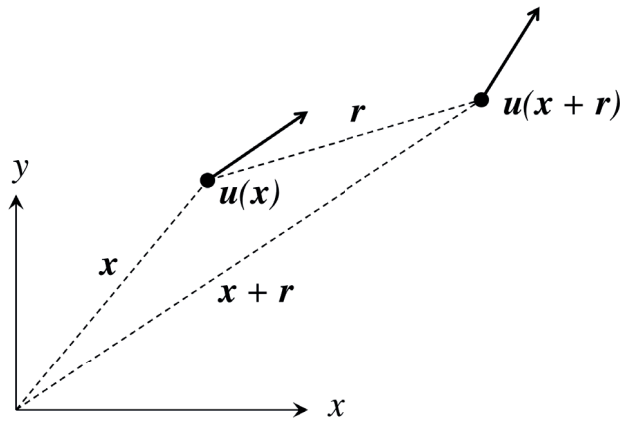

Figure 2.3: The two-point velocity correlation $R_{ij}(\boldsymbol{x}, \boldsymbol{r})$ measures the correlation between the velocity at location $\boldsymbol{x}$ and $\boldsymbol{x} + \boldsymbol{r}$.

Two-point correlations measure how well a flow field (signal) is correlated

with itself over a displacement $\boldsymbol{r}$. Commonly the normalization

$$K_{ij}(\boldsymbol{x}, \boldsymbol{r}) = \frac{R_{ij}(\boldsymbol{x}, \boldsymbol{r})}{R_{ij}(\boldsymbol{x}, 0)}$$

is employed to give the *correlation coefficient* (or correlation function), K_{ij}, which is unity at zero separation. The correlation coefficient decreases as $\boldsymbol{r}$ increases, and eventually it goes to zero ($K_{ij} \to 0$ as $r \to \infty$). The integral scale of turbulence is related to the two-point correlation by

$$L_k^{ij}(\boldsymbol{x}) = \int_0^\infty K_{ij}(\boldsymbol{x}, r_k)\, \mathrm{d}r_k.$$

Here, $L_k^{ij}(\boldsymbol{x})$ is the length scale in direction k at position $\boldsymbol{x}$, based on the correlation between velocity components i and j.

The two-point correlation is closely related to another measure of non-local flow statistics: The turbulence energy spectrum, i.e. the power spectral density of the turbulent velocity field, occasionally referred to as the power, frequency or velocity spectrum, can be formally defined as

$$E_{ij}(\boldsymbol{\kappa}) = \frac{1}{(2\pi)^3} \iiint_{-\infty}^{\infty} R_{ij}(\boldsymbol{r}) e^{i\boldsymbol{\kappa}\cdot\boldsymbol{r}}\, \mathrm{d}^3\boldsymbol{r}, \tag{2.9}$$

for homogeneous, statistically steady turbulence. Here, $\boldsymbol{\kappa} = (\kappa_1, \kappa_2, \kappa_3)$ is the wavenumber vector.

The turbulence spectrum quantifies the amount of energy contained per wavenumber – or, equivalently, wavelength – in a turbulent flow. As such, it contains information about the range of length scales in the flow, as well as which length scales are associated with what portion of the total energy.

An equivalent turbulence energy spectrum function, in which directional information is removed, is often used. Several forms are used in the literature, such as the spherically symmetric form of Durbin and Petterson Reif (2011, p. 256):

$$E(\kappa) = 2\pi E_{ii} \kappa^2, \tag{2.10}$$

where $\kappa = |\boldsymbol{\kappa}|$ is the magnitude of the wavenumber vector.

In channel flow (see Section 5), the one-dimensional spectrum is usually measured, corresponding to E_{ij} integrated over two wavenumber directions. Equivalently, the spectrum, which is now a function of z, can be computed from the unidirectional correlation function, i.e. for the streamwise direction

$$E_{ij}(z,\kappa_1) = \frac{1}{2\pi}\int_{-\infty}^{\infty} R_{ij}\big(z,(r_1,0,0)\big)e^{i\kappa_1 r_1}\,\mathrm{d}r_1. \tag{2.11}$$

By the Wiener-Khinchin theorem (Bendat and Piersol, 1980, p. 55), Eq. (2.11) is equivalent to the power spectrum of the streamwise velocity signal. Note also that spectra of other flow fields can be computed in similar manners.

Kolmogorov (1941a) used dimensional arguments to show that for high Reynolds-number flows, the energy spectrum should contain a range of wavenumbers, denoted the *inertial subrange*, in which

$$E_k \sim \varepsilon^{2/3}\kappa^{-5/3}.$$

In the inertial subrange, energy is neither created nor destroyed. It is only transferred from larger scales down towards the smaller scales, where it is subsequently dissipated. A larger inertial subrange implies a larger separation of turbulence scales, i.e. flows with a higher Reynolds number. Kolmogorov's inertial subrange scaling has been confirmed in experiments with high Reynolds-number turbulence (Grant et al., 1962; Saddoughi and Veeravalli, 1994).

From Kolmogorov's dimensional arguments, it follows that the smallest scales of the flow are defined by

$$\eta = \left(\frac{\nu^3}{\varepsilon}\right)^{1/4},$$
$$\tau_K = \left(\frac{\nu}{\varepsilon}\right)^{1/2},$$

where η and τ_K are the Kolmogorov length and time scales, respectively. From these scales, a Kolmogorov velocity scale can also be formed. The Kolmogorov length scale can also be defined as a vector in the case of local anisotropy, by using components of the dissipation rate tensor, ε_{ij}.

Whereas the integral scales are located at the low-wavenumber end of the

energy spectrum, the Kolmogorov scales are at the high-wavenumber end of the spectrum. It can be shown that the turbulent Reynolds number, Re_t, is related to the ratio between them, i.e.

$$\mathrm{Re}_t \equiv \frac{L_t U_t}{\nu} \sim \left(\frac{L_t}{\eta}\right)^{4/3},$$

in which $L_t \sim \max\left(L_k^{ij}\right)$ and U_t represent typical length and velocity scales of the largest turbulent eddies of the flow.

Figure 2.4 illustrates a typical energy spectrum for a high Reynolds-number turbulent flow.

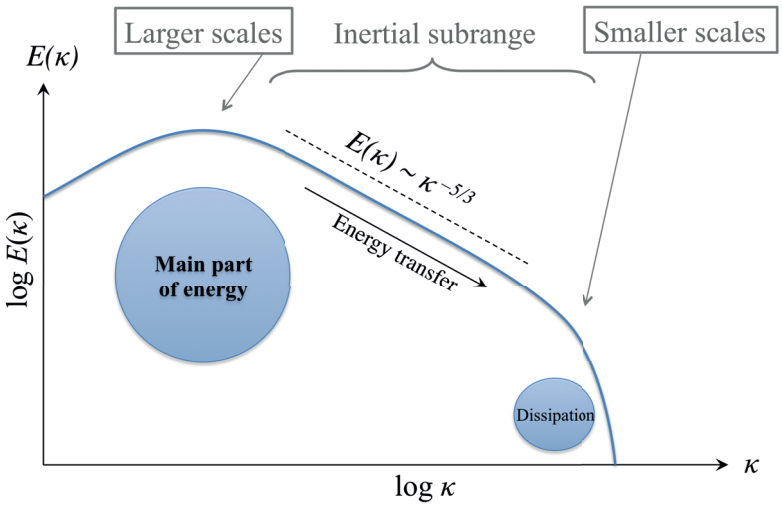

Figure 2.4: Schematic of the turbulence energy, $E(\kappa)$, as a function of wavenumber, κ, for high-Re turbulence.

2.4 Turbulence structures

As illustrated in Figure 2.5, turbulent flows clearly exhibit some form of organized structure; eddies of various scales can usually be identified, and sweeps and bursts of fluid can occasionally be observed. Any flow region of finite spatial and temporal extent with a characteristic, coherent flow pattern can be referred to as a coherent structure or a *turbulence structure*.

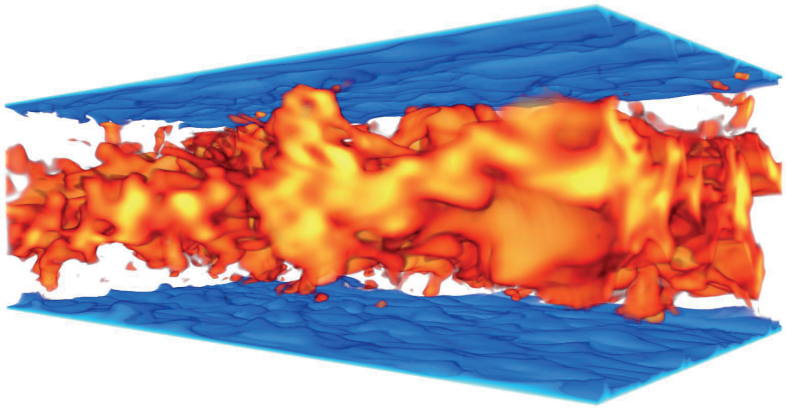

Figure 2.5: Three-dimensional visualization of instantaneous streamwise velocity in flow between two parallel plates. The blue-colored isosurfaces indicate low-velocity regions near the wall; the isosurface in red (yellow) indicates the core region of high (and very high) velocity. Flow is from left to right.

The interest in turbulence structures have several motivations, apart from a desire to seek order and regularity: Turbulence structures can help explain visual flow patterns dynamically, and seemingly complex mechanisms may thus be explained in terms of elemental structures. Furthermore, the identification of structures might be useful in classifying turbulent flows and appreciating different flow regimes. From a more practical point of view, increased understanding of turbulence structures may lead to the ability to modify them, for example to reduce

drag or trigger transitions, and it can inspire the foundation of improved turbulence models.

Kline and Robinson (1990); Robinson (1991) give an overview of the most well-known structures, including low-speed streaks in the viscous region, ejections and sweeps of wall-bounded flows, various vortical structures, such as rolls, sheets, and hairpin (or horseshoe) vortices, shear layers, pockets, backs and various large-scale motions. Structures specifically related to wall-bounded turbulence are treated in detail by e.g. Panton (2001), whereas structures related specifically to turbulence transition are summarized by White (2006, p. 370), among others.

According to Pope (2000, p. 324), a number of techniques are available to identify flow structures, such as single-point measurements combined with quadrant analysis or variable-interval time averaging, pressure measurements, velocity gradient tensor invariant analysis, or proper orthogonal decomposition.

DNS, and to some extent LES, is very well suited to the task of capturing the entirety or a subset of turbulence structures. The analysis can then be based on the full four-dimensional flow field, and data extraction can be performed non-intrusively. Recent advances in computer visualization (McLoughlin et al., 2010) provide the means to inspect such vast amounts of simulation data visually in order to intuitively identify and observe complex turbulence structures.

Given the complex spatiotemporal nature of turbulent structures, they are difficult to quantify. Some of the measures discussed in the previous section, such as energy spectra, can be used to indicate certain structural characteristics, but in general, visual inspection is still of major importance in the context of turbulent flow structures. However, a few additional routes to quantitatively identify or measure the structure of turbulence will be discussed briefly in the following.

Vortical structures are closely connected to the structural state of a turbulent flow. The vorticity of the velocity field is given by

$$\tilde{\omega}_i = \epsilon_{ijk} \partial_j \tilde{u}_k, \tag{2.12}$$

in which ϵ_{ijk} is the cyclic permutation tensor; $\epsilon_{ijk} = 1$ for $ijk = \{123, 231, 312\}$, $\epsilon_{ijk} = -1$ for $ijk = \{321, 213, 132\}$, and $\epsilon_{ijk} = 0$ otherwise.

The most intuitive way of visualizing vorticity is perhaps by its magnitude,

the so-called *enstrophy*, $|\tilde{\boldsymbol{\omega}}|$. A drawback of the enstrophy as a tool to characterize vortices is that it measures all regions of vorticity, including so-called vortex sheets. More sophisticated quantifications of vorticity structures include the second invariant of the velocity gradient matrix (Hunt et al., 1988) and the $\lambda_2 < 0$ criterion of Jeong and Hussain (1995). These methods are well-suited to identify vortex cores, tubes and other vortical structures. However, through its dependence on velocity gradients, vorticity is generally associated with small-scale flow structures of low energy. Hence, turbulence structures identified from the vorticity field are not necessarily the most dynamically important structures of a turbulent flow, since their energy can be considered small compared to the energy of integral-scale structures.

More recently, single-point *structure tensors* have been utilized to elucidate the energetic large-scale structures of turbulent flows. Although concepts such as dimensionality had been used previously, Kassinos and Reynolds (1995) was the first to formally introduce the complete structure tensor framework. Their group at Stanford is also working towards development of structure-based turbulence models (cf. e.g., Kassinos et al., 2000; Pecnik et al., 2012). However, except for the prototypical flows reported by Kassinos et al. (2001) and a few other cases (Reif et al., 2002; Helgeland et al., 2005; Bhattacharya et al., 2008), the structure tensor approach to structure characterization as a means of describing the turbulence remains largely unexplored. In the present thesis, several physically meaningful implications of the quantitative information inherent in the structure tensors are discussed.

Analogously to the full vorticity field, Eq. (2.12), the fluctuating vorticity is defined as $\omega_i = \epsilon_{ijk}\partial_j u_k$. Based on ω_i, a fluctuating vector stream function, ψ_i, can be computed from the Poisson equation,

$$\partial_k \partial_k \psi_i = -\omega_i. \tag{2.13}$$

The fluctuating stream function also satisfies $\partial_i \psi_i = 0$. The fluctuating velocity field can be retrieved from ψ_k via $u_i = \epsilon_{ijk}\partial_j \psi_k$. That is, the stream function is a vector potential of the velocity field.

Following Kassinos et al. (2001), a family of single-point correlation tensors, carrying non-local information, can be defined from products of the fluctuating

stream-function gradients:

$$D_{ij} = \langle \partial_i \psi_k \partial_j \psi_k \rangle \qquad \text{(Dimensionality)}$$
$$F_{ij} = \langle \partial_k \psi_i \partial_k \psi_j \rangle \qquad \text{(Circulicity)}$$
$$C_{ij} = \langle \partial_k \psi_i \partial_j \psi_k \rangle \qquad \text{(Inhomogeneity)}$$
$$Q_{ijk} = -\langle u_j \partial_k \psi_i \rangle. \qquad \text{(Stropholysis)}$$

These large-scale tensors contain structural information about the turbulence in a fluid flow field and are referred to as *structure tensors*. Together with the Reynolds stress tensor, they form a tensorial base for a complete one-point theory of turbulence (Kassinos et al., 2001). The structure tensors are not independent, i.e.

$$\langle u_i u_j \rangle + F_{ij} + D_{ij} + C^*_{ij} = q^2 \delta_{ij}, \tag{2.14}$$

in which $C^*_{ij} = C_{ij} + C_{ji}$, $q^2 = \langle u_i u_i \rangle$, and δ_{ij} is the Kronecker delta. The different tensors have distinct physical interpretations:

The dimensionality tensor, D_{ij}, carries information about the spatial variation of large-scale turbulence structures. In particular, it expresses the level of two-dimensionality of the structures. Even if D_{ij} represents a one-point correlation, the tensor carries non-local information about the structure of turbulence, which can be seen from the elliptic nature of Eq. (2.13). Assuming statistical homogeneity for the sake of clarity, one can write D_{ij} in wavenumber space (Kassinos and Reynolds, 1995),

$$D_{ij} = \int \frac{\kappa_i \kappa_j}{\kappa^2} E_{nn}(\boldsymbol{\kappa}) \, \mathrm{d}^3 \boldsymbol{\kappa}.$$

Here, $\boldsymbol{\kappa} = (\kappa_1, \kappa_2, \kappa_3)$ is the wavenumber vector (with κ its squared norm). $E_{ij} \equiv \hat{u}_i(\boldsymbol{\kappa}) \hat{u}^*_j(\boldsymbol{\kappa})$ is the velocity spectrum tensor, in which hats $\hat{(\cdot)}$ denote Fourier coefficients and the asterisk $(*)$ denotes complex conjugation. The spectral representation of D_{ij} thus depends on the wavenumber vector, κ_i, which contains length scale directionality and magnitude information. For example, if if $\kappa_i = 0$, the structure does not vary in the x_i-direction.

In physical space, the dimensionality tensor is directly related to the two-point

correlation tensor via (Bhattacharya et al., 2008)

$$D_{ij} = -\frac{1}{4\pi} \int_{\mathbb{R}^3} \frac{1}{|\boldsymbol{r}|} \frac{\partial^2 R_{kk}(\boldsymbol{r})}{\partial r_i \partial r_j} \, \mathrm{d}\boldsymbol{r}. \tag{2.15}$$

For idealized ellipsoidal structures, the average volume of the structures can be defined by means of the integral length scales in each of the three principal directions of the ellipsoid, i.e. $V_s \propto \mathcal{L}_1\mathcal{L}_2\mathcal{L}_3$, where $\mathcal{L}_i$ are the integral length scales in the directions of the principal axes. It can be shown that Eq. (2.15) implies that $V_s \propto 1/(D_{11}D_{22}D_{33})$ when D_{ij} is expressed in principal axes. The dimensionality tensor is thus closely connected to the spatial extent of the turbulence structures.

The circulicity tensor, F_{ij}, is perhaps most easily interpreted as a large-scale vorticity measure. By considering the Fourier transform, $\mathcal{F}[\cdot]$, of the circulicity tensor, using the assumption of homogeneity, it follows that

$$\mathcal{F}[F_{ij}] = \kappa^2 \langle \hat{\psi}_i \hat{\psi}_j^* \rangle = \frac{\langle \hat{\omega}_i \hat{\omega}_j^* \rangle}{\kappa^2},$$

i.e. its wave components are similar to those of the vorticity tensor multiplied by a factor $1/\kappa^2$. This effectively diminishes the contributions of smaller scales. The last equality above follows from the Fourier transformation of Eq. (2.13).

The spectral representations of the dimensionality and circulicity tensors are equivalent to the physical-space interpretations of the tensors, and the assumption of homogeneity above is for convenience only.

The inhomogeneity tensor, C_{ij}, represents the deviation from homogeneity of the turbulence field. The incompressibility condition ($\partial_k \psi_k = 0$) implies that the tensor can be rewritten $C_{ij} = \partial_k \langle \psi_i \partial_j \psi_k \rangle$ and is thus identically zero in homogeneous turbulence. It should be noted that C_{ij} is not symmetric.

Figure 2.6 illustrates schematically some examples of idealized structures and the corresponding structure tensors.

As discussed in Paper IV, even though the connections between the two-point velocity correlation tensor, the integral length scales, the energy spectra and the structure tensors are far from trivial, it is important to appreciate that they are all closely related to the spatial coherence (i.e. the spatial structure) of the turbulence. As such, they are different beasts entirely from one-point measures.

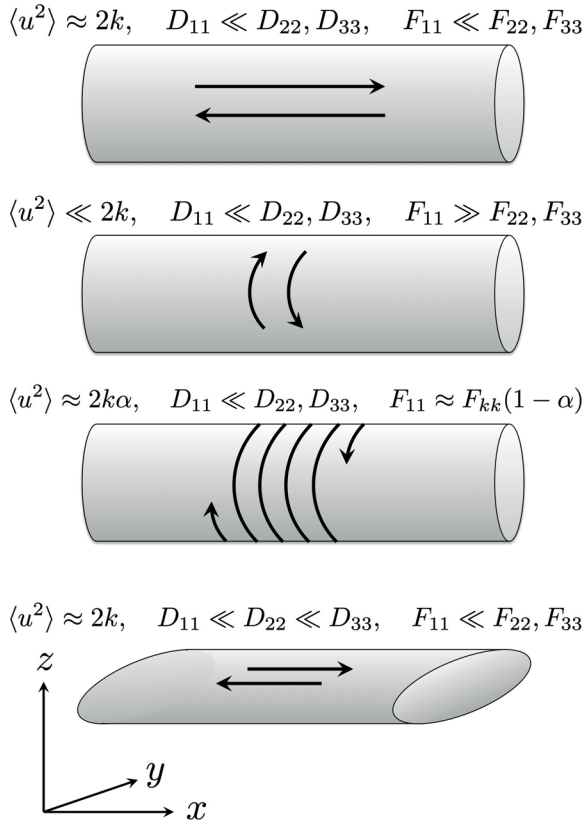

Figure 2.6: Conceptual diagram showing selected combinations of structure tensor component values and corresponding idealized structures. Figure adapted from Paper IV.

2.5 Large-eddy simulation

The LES methodology arose from needs in meteorology; whereas DNS was by far too computationally demanding to be of use in real-life applications, RANS models were too inaccurate and case-dependent. LES resolves some portion of the turbulence spectrum, thus seeking a solution in-between DNS and RANS in terms of level of detail.

Although first formulated by Lilly (1967) and then applied by Deardorff (1970), it was not until a few decades ago that the advances in computing power made LES a common research tool. Very coarse LES-like simulations had been performed as early as the 1950s (Charney et al., 1950; Phillips, 1956), but without explicitly modeling the unresolved scales[2].

There are several routes to obtaining the LES equations and interpreting their implications, depending on whether one takes a more mathematical, numerical, or physical approach. The text books by Pope (2000); Lesieur (2005); Sagaut (2006); Wyngaard (2010) provide thorough treatments of the subject.

The basis of LES is the decomposition of fluid flow fields into *resolved* and *subgrid* (unresolved) parts, e.g. $\tilde{u}_i^r(\boldsymbol{x}, t)$ and $\tilde{u}_i^s(\boldsymbol{x}, t)$, respectively, for the velocity field. Formally, the decomposition is obtained via a *filtering operation*, in which the field, say, $\tilde{u}_i(\boldsymbol{x})$, is filtered by a filter function, $G(\boldsymbol{x})$, via the convolution

$$\tilde{u}_i^r(\boldsymbol{x}) = \int_{-\infty}^{\infty} G(\boldsymbol{x} - \boldsymbol{r})\tilde{u}_i(\boldsymbol{x})\,\mathrm{d}\boldsymbol{r},$$

to produce the resolved field, $\tilde{u}_i^r$ and the subgrid field $\tilde{u}_i^s = \tilde{u}_i - \tilde{u}_i^r$.

The Fourier transform of a filter function is its associated transfer function, which represents the corresponding filtering in spectral space. The most common filter in LES algorithms based on the FVM is an implicit running-mean filter, where the spatial averaging size directly depends on the size of the local computational cell. In spectral LES codes, a wave cutoff filter is commonly used instead.

A filter function used in LES should satisfy conservation of constants, commutation with derivation, and be a linear operator (Sagaut, 2006, p. 17). In gen-

[2]It reveals a lot about the state of numerics at the time that punch card were used for computations, and that J. G. Charney writes in his 1950 paper "[The solution algorithm] is not, however, recommended for hand computation".

eral, however, filters are not Reynolds operators. That is, a filtered (resolved) variable does not necessarily pass unchanged through the filter, and the filter of a subgrid variable is not necessarily zero.

Regardless of the specifics of the filter function, the filtered – i.e. the resolved – conservation equations for momentum, mass, and scalars can be formulated

$$\partial_t \tilde{u}_i^r + \tilde{u}_k^r \partial_k \tilde{u}_i^r = -\frac{1}{\rho}\partial_i \tilde{p}^r + \nu \partial_k \partial_k \tilde{u}_i^r - \partial_k \tau_{ik} + F_{V,i}, \tag{2.16}$$

$$\partial_k \tilde{u}_k^r = 0, \tag{2.17}$$

$$\partial_t \tilde{c}^r + u_k^r \partial_k \tilde{c}^r = \gamma \partial_k \partial_k \tilde{c}^r - \partial_k f_k, \tag{2.18}$$

in which $\tau_{ik} = (\tilde{u}_i \tilde{u}_k)^r - \tilde{u}_i^r \tilde{u}_k^r$ and $f_k = (\tilde{c}\tilde{u}_k)^r - \tilde{c}^r \tilde{u}_k^r$ represent the unresolved and thus unknown *subgrid stresses* and *scalar subgrid fluxes*, respectively. In other words, these terms require modeling.

Note the resemblance of Eq. (2.16)–(2.18) to Eqs. (2.1)–(2.3). In Eq. (2.16), it is assumed that the volume force $F_{V,i}$ passes through the filter unchanged.

The solution of Eqs. (2.16)–(2.18) yield resolved velocity, pressure and scalar fields. These fields are generally three-dimensional, time-dependent approximations to the full flow fields and can thus be subjected to Reynolds decomposition, e.g. $\tilde{u}_i^r = U^r + u^r$ for the velocity field, in order to compute flow field statistics.

2.5.1 Subgrid-viscosity models

The most common class of subgrid-stress models are subgrid-viscosity models, akin to the Boussinesq eddy-viscosity hypothesis originally used within the RANS modeling framework. Lilly (1967) introduced first-order and second-order derivations of the subgrid-viscosity, and the former, now known as the Smagorinsky model, is still widely used, albeit often in modified forms. A thorough treatment of numerous other modeling techniques can be found in e.g. Sagaut (2006).

Lilly (1967) assumed that the subgrid stresses were proportional to the resolved strain rate and suggested that Smagorinsky's (1963) eddy-viscosity form be used. In present-day terminology, that implies that

$$\tau_{ij}^{\text{Lilly}} = -2\nu_s \tilde{s}_{ij}^r, \tag{2.19}$$

where the subgrid viscosity $\nu_s(\boldsymbol{x}, t) = (C_d L_\Delta)^2 \sqrt{2\tilde{s}^r_{ij}\tilde{s}^r_{ij}}$, in which L_Δ is the LES filter width, C_d is the Smagorinsky coefficient, and $\tilde{s}^r_{ij} = (1/2)(\partial_j \tilde{u}^r_i + \partial_i \tilde{u}^r_j)$ is the resolved strain rate.

In practice, L_Δ is implicitly determined by the local computational cell size in most FVM solvers. The filter width, and consequently the cell sizes, should always be at least small enough to ensure that the spatial filter corresponds to a spectral filter which do not affect wavenumbers below the inertial subrange. The Smagorinsky model, defined by Eq. (2.19), uses no explicitly specified filter. However, in the case of isotropic turbulence, the model implies a unique filter which in many respects behave like a Gaussian filter (Pope, 2000, p. 590).

In FVM-based LES solvers, the scalar subgrid flux, f_i, is frequently modeled similarly to the momentum subgrid stresses, i.e. by a subgrid-diffusivitiy model of the form $f_i = \gamma_s \partial_i \tilde{\theta}$. Here, γ_s is the subgrid diffusivity, for which various models exist, such as the very common relation $\gamma_s = \nu_s / \mathrm{Pr}_s$, where the subgrid turbulent Prandtl number lies in the range $0.1 \leq \mathrm{Pr}_s \leq 1$ in the literature, with $\mathrm{Pr}_s = 0.6$ being typical (Sagaut, 2006, p. 463). Dynamic models for the subgrid Prandtl number also exist.

The original Smagorinsky model suffers from the fact that the Smagorinsky coefficient inherently depends on the flow regime, from zero in laminar flow to about $C_d \approx 0.15$ in high-Reynolds number turbulence (Pope, 2000, p. 619). The *dynamic* Smagorinsky model resolves this issue by determining a suitable local value of the coefficient. The model, proposed by Germano et al. (1991), can be outlined as follows (for convenience, the tilde symbols denoting full instantaneous fields are dropped for the time being):

Given a subgrid-viscosity model,

$$\tau_{ij} = 2C_d L^2_\Delta |s^r| s^r_{ij},$$

in which $|s^r| = \sqrt{2 s^r_{ij} s^r_{ij}} = 2C_d \alpha_{ij}$, and the superscript r denotes resolved (filtered) variables as usual, with the associated filter width L_Δ, a second model can be defined as

$$\tau^*_{ij} = 2C_d L^2_{\Delta *} |s^{r*}| s^{r*}_{ij} = 2C_d \beta_{ij}.$$

Here, the superscript $r*$ denotes a second LES filter, with an associated filter size $L_{\Delta *}$. The second filter is usually referred to as a *test filter*, and its filter size is

often around twice the size of the ordinary filter.

Now, letting $L_{ij} = u_i^{r*}u_j^{r*} - (u_i^r u_j^r)^{r*}$, the properties of the LES filter implies that

$$-L_{ij} = \tau_{ij}^* - (\tau_{ij})^{r*},$$

referred to as *Germano's identity*. Furthermore,

$$\begin{aligned} -L_{ij} &= 2(C_d\beta_{ij} - (C_d\alpha_{ij})^{r*}) \\ L_{ij} &\approx 2C_d(\alpha_{ij}^{r*} - \beta_{ij}) \\ &= 2C_d L_\Delta^2 M_{ij} \\ C_d &= \frac{L_{ij}}{2L_\Delta^2 M_{ij}}, \qquad \text{(no summation on } i,j) \end{aligned}$$

where $M_{ij} = (L_{\Delta*}/L_\Delta)^2|s^{r*}|s_{ij}^{r*} - (|s^r|s_{ij}^r)^{r*}$. To improve the robustness of Germano's model, Lilly (1992) introduced a normalization and local spatial averaging procedure according to

$$C_d = \frac{1}{2L_\Delta^2}\frac{\langle L_{ij}M_{ij}\rangle}{\langle M_{rs}M_{rs}\rangle},$$

which is the basis for most dynamic Smagorinsky models presently in use.

Despite the advantages of LES in predicting details of turbulent flows, near-wall treatment at high Reynolds numbers remains a challenge. At lower Reynolds numbers, the viscous, high-shear region close to solid boundaries may be fully resolved, as in DNS, but for most real-life flows, this is unfeasible. If wall-generated shear is the main instigator of turbulence, near-wall modeling akin to RANS wall models must be employed to obtain reasonable results. However, if other turbulence sources dominate, e.g. jets, vortex shedding, or shear from geometric roughness, LES may be well-suited.

A final concern regarding LES, shared with DNS, is that of appropriate boundary conditions, particularly in the case of velocity inlets or free-stream boundaries. The prescription of physically realistic conditions consistent with the mathematical models and numerical implementation of a solver is still an area of active research, cf. e.g. Keating et al. (2004).

2.5.2 The LES-RSTE with subgrid-viscosity modeling

When a system of filtered conservation equations, Eqs. (2.16)–(2.18), is solved, the resulting fields are resolved approximations to the solution of the system of the "full" conservation equations, i.e. Eqs. (2.1)–(2.3). As such, the fields can be subjected to the same Reynolds decompositions as the full fields, as well as subsequent analysis. In particular, the RSTE and the TKETE can be derived for the resolved fields.

The subgrid-viscosity model of Eq. (2.19) can be substituted into the filtered momentum conservation equation. Then, the usual "RANS procedure" follows (Section 2.2): Resolved Reynolds decompositions are inserted, the equation is averaged, and the average equation is subtracted from the instantaneous equation. The resulting equation for u_i^r (resolved fluctuating velocity) are multiplied by u_j^r and added to the same equation for u_j^r multiplied by u_i^r. The final result is then averaged to produce the RSTE with LES model effects included, i.e. Eq. (2.4) with some additional terms.

The additional terms in the LES-RSTE follow from the fact that the subgrid viscosity is not constant, but rather depends on the random and stochastic resolved strain rate and filter size (i.e. local computational cell size). Hence, its Reynolds decomposition, $\tilde{\nu}_s = \overline{\nu}_s + \nu_s$, must also be substituted into the filtered momentum equation before averaging. The additional terms associated with the subgrid-viscosity are required for the resolved Reynolds stress budget to balance. Dropping the superscript r, the RSTE for the resolved Reynolds stresses is similar to Eq. (2.4), but contains the following additional terms on the right-hand side:

$$\begin{aligned} &- 2\overline{\nu}_s\langle\partial_k u_i \partial_k u_j\rangle + \overline{\nu}_s\partial_k\partial_k\langle u_i u_j\rangle \\ &+ \langle u_i\partial_k\nu_s\rangle\partial_k U_j + \langle u_j\partial_k\nu_s\rangle\partial_k U_i \\ &+ \langle\nu_s u_i\rangle\partial_k\partial_k U_j + \langle\nu_s u_j\rangle\partial_k\partial_k U_i \\ &+ \partial_k\overline{\nu}_s\partial_k\langle u_i u_j\rangle. \end{aligned} \tag{2.20}$$

The first term represents what is commonly referred to as a subgrid dissipation term for the Reynolds stresses. The second term corresponds to subgrid diffusion. The other terms have no clear physical interpretations, but their forms imply that the terms on the second line may be referred to as subgrid production, the terms

on the third line may be called subgrid transport, and the term on the fourth line may be denoted subgrid advection.

Analogously to the RSTE, the transport equations for e.g. temperature variance, scalar fluxes, or higher-order moments of such quantities will contain subgrid terms when derived in an LES context. The procedure above can be carried out for different kinds of LES models or in a more general way, using $\tau_{ij}(\boldsymbol{x}, t)$.

As the resolution of an LES increases, the subgrid terms diminish, and in the limit of DNS resolution, the terms should ideally tend to zero. However, depending on both the subgrid model and the numerical algorithm, this is not always the case, cf. also Section 6.2. FVM-based LES methods with filtering sizes based on mesh resolution (such as Smagorinsky-based models) are inherently highly mesh-dependent, in contrast to most RANS models which tend to a unique model solution as long as the computational mesh is "fine enough".

Chapter 3

Stratified flows

A stratified (from Latin *stratum*, meaning "layer") fluid is a fluid in which an overall density gradient is present, typically caused by differences in temperature or salinity. Usually, the term refers to stratified flows in which the density gradient is parallel (or nearly parallel) to the gravitational acceleration and perpendicular (or nearly perpendicular) to the mean flow direction.

In a stably stratified flow, lighter fluid lies on top of heavier fluid, i.e. the density increases in the direction of gravity. The stratification may be continuous, but distinct layers of different densities may also form - particularly in the case of large density differences. Stable stratification is so called since the configuration is self-preserving in the sense that small flow field perturbations are dampened and do not change the state of the system.

If a parcel of fluid in continuously stable stratified flow is vertically displaced a small distance away from its equilibrium position, it will oscillate back towards its original location. The parcel will gain enough kinetic energy to "overshoot", i.e. pass its equilibrium position, and will so oscillate back and forth with decaying amplitude until it ends up at rest at its original location. The oscillations will have a frequency equal to the Brunt-Väisälä frequency, to be defined shortly.

The reverse case of heavier fluid on top of lighter fluid is referred to as unstable stratification; small perturbations are amplified, and there is intense vertical exchange of momentum in the fluid, as opposed to the stable case, where vertical mixing is inhibited.

In the present thesis, stable stratification will be in focus; stable stratifica-

tion affects anisotropy, energy transfer, and turbulence structures in ways not yet completely clear (Wyngaard, 2010; Mahrt, 2014). The dynamics of stable stratification is less robust than neutral or unstably stratified flows; at high levels of stable stratification, turbulence may be extinguished, either within large patches of fluid or totally (García-Villalba and del Alamo, 2011; Flores and Riley, 2011; Mahrt, 2014).

Another motivation for the study of stably stratified flow concerns the dispersion of gases and aerosols, which is significantly altered under imposed stable stratification; vertical turbulent diffusion typically decreases, leading to higher concentrations further downstream (cf. Paper III). Moreover, geometric barriers (buildings, hills, walls) may keep high-concentration regions contained for extended periods of time.

3.1 The Boussinesq approximation

For low-Mach number flows (with typical flow speeds less than approximately 0.3 times the speed of sound) with small variations in hydrostatic pressure and in which pressure wave propagation is unimportant, compressibility effects are insignificant (Kundu and Cohen, 2008). According to Boussinesq (1903), density changes in the fluid caused by temperature variations can then be neglected except in the gravity term, where ρ is multiplied by g, provided that the temperature differences are small.

These assumptions lead to the Boussinesq approximation, i.e. a modified form of the incompressible momentum equation (2.1), together with a transport equation for temperature, $\tilde{\theta} = \tilde{\theta}(\boldsymbol{x}, t)$, of the form (2.3), which arises from the (compressible) energy equation.

A limit on the temperature variation can be estimated from the compressible mass conservation equation, which can be expressed

$$\frac{1}{\tilde{\rho}} \frac{\mathrm{D}\tilde{\rho}}{\mathrm{D}t} + \partial_i \tilde{u}_i = 0, \tag{3.1}$$

to separate the density and velocity fields into separate terms. Here $\mathrm{D}\tilde{\rho}/\mathrm{D}t = \partial_t \tilde{\rho} + \tilde{u}_i \partial_i \tilde{\rho}$ is the material derivative of density, $\tilde{\rho}(\boldsymbol{x}, t)$. Comparing the two terms

of Eq. (3.1) with an order-of-magnitude analysis yields

$$\frac{(1/\tilde{\rho})(\mathrm{D}\tilde{\rho}/\mathrm{D}t)}{\partial_i \tilde{u}_i} \sim \frac{(1/\rho)(U\delta\rho/L)}{U/L} = \frac{\delta\rho}{\rho}, \tag{3.2}$$

in which U, ρ, and $\delta\rho$ are typical velocity and density scales, and a typical density *change* over a distance L, respectively. For the Boussinesq approximation to hold, i.e. for Eq. (2.2) to be a good approximation of Eq. (3.1), the ratio in Eq. (3.2) should be small, i.e. $\delta\rho/\rho \ll 1$ is required.

The approximation also encompasses the assumption that relative density changes scale linearly with changes in temperature, i.e.

$$\frac{\delta\rho}{\rho} = -\alpha\delta\Theta, \tag{3.3}$$

where $\alpha = -\tilde{\rho}^{-1}(\partial\tilde{\rho}/\partial\tilde{\theta})_p$ is the thermal expansion coefficient of the fluid (at constant pressure), and $\delta\Theta$ is a typical temperature change. The requirement of "small" temperature changes can be written as

$$\alpha\delta\Theta \ll 1.$$

For ideal gases, $\alpha \sim 1/\Theta_0$, where Θ_0 is a typical fluid temperature, so the Boussinesq approximation holds as long as $\delta\Theta \ll \Theta_0$. Hence, for example, fluid flow in the atmosphere including effects of temperature variations ($\pm$ 10 K in an environment at 300 K) can be modeled as an incompressible fluid flow with the Boussinesq approximation – provided that the vertical scale does not exceed $\sim$ 10 km, at which point compressibility effects from hydrostatic pressure differences become important.

As seen from Eq. (3.3), density and temperature are equivalent active-scalar fields in Boussinesq flows. Similarly, thermal stratification and density stratification describe the same phenomenon. In the present thesis, the temperature field is generally used to incorporate effects of stratification.

3.2 Governing equations of stratified flow

The governing equations of incompressible flow with density variations satisfying the requirements for the Boussinesq approximation are similar to Eq. (2.1)–(2.2). The effects of buoyancy can be included as a volume force in Eq. (2.1), i.e.

$$F_{V,i} = \frac{\rho'}{\rho} g_i,$$

in which $\rho' = \rho'(\boldsymbol{x}, t)$ is the *reduced density*, ρ is a (constant) reference density, and $g_i = (0, 0, -g)$ is the gravitational acceleration. The reduced density incorporates the density deviation from its reference state, i.e. the local, instantaneous equivalent of the $\delta\rho$ scale in the preceding section.

From Eq. (3.3), it follows that

$$\frac{\rho'}{\rho} = -\alpha\theta',$$

where $\theta' = \tilde{\theta} - \Theta_0$ is the deviation in temperature from its reference state. The effects of buoyancy can thus be expressed in terms of temperature differences, i.e.

$$F_{V,i} = -\alpha g_i \left(\tilde{\theta} - \Theta_0\right).$$

Assuming that the fluid behaves as an ideal gas under small density changes and that Fick's law of heat conduction holds, it can be shown from the thermal energy equation that the transport equation for temperature is identical to that of a scalar (Kundu and Cohen, 2008, p. 127), i.e. Eq. (2.3) with $\tilde{c} = \tilde{\theta}$. In this case the molecular diffusivity is given by $\gamma \equiv k_c/\rho C_p$, where k_c and C_p are the thermal conductivity and specific heat (at constant pressure) of the fluid, respectively, all assumed to be constant).

Heating due to viscous dissipation of kinetic energy is excluded from this equation, since an order-of-magnitude analysis shows that the heating term would be extremely small ($\sim 10^{-7}$) for most real flows (Reif and Andreassen, 2003).

As for any other turbulent field, the temperature can be decomposed into mean and fluctuating parts, viz. $\tilde{\theta} = \Theta + \theta$, and filtered equations for LES can be derived. Turbulent fluid flows with the Boussinesq approximation can be modeled by an

LES equation set of the form of Eqs. (2.16)–(2.18) with $F_{V,i} = \alpha g_i \left(\tilde{\theta}^r - \Theta_0 \right)$ and $\tilde{c}^r = \tilde{\theta}^r$.

The inclusion of an additional source term in the momentum conservation equation also has consequences for higher-order moments. When deriving the RSTE, Eq. (2.4), an additional buoyancy destruction term,

$$G_{ij} = -\alpha \left[g_i \langle u_j \theta \rangle + g_j \langle u_i \theta \rangle \right],$$

appears on the right-hand side.

3.3 Effects of imposed stable stratification on turbulent flow

Stable stratification generally inhibits the development or sustainability of turbulence, in large part due to reduced vertical mixing. The latter fact also implies a change in turbulence length scales – and, more generally, a change of turbulence structures – of the flow under imposed stratification. This is one of the main topics in both Paper II and Paper IV.

Additionally, since the buoyancy forcing acts in the vertical direction only, stratification introduces large-scale anisotropies in the flow. It has been shown (Thoroddsen and Van Atta, 1992; Smyth and Moum, 2000; Reif and Andreassen, 2003) that such anisotropies are commonly present at smaller turbulence scales as well, a topic discussed more thoroughly in Papers I and II.

Finally, the Reynolds stress and turbulence kinetic energy budgets can be severely altered by stratification, i.e. the flow dynamics can change significantly, as illustrated by the inclusion of the buoyancy destruction term in Section 3.2. This change in dynamics is investigated in Papers II and III.

The practical implications of the above phenomena are numerous: The kinematic structure of the flow will change, with associated changes in spatial and temporal scales. Hence, dispersion of contaminants may also be severely affected. Section 4 exemplifies consequences of stratification in the context of the stable atmospheric boundary layer, whereas Section 5.2 discusses implications for channel flow.

The interplay between stratification and turbulence is commonly characterized by the Richardson number. The gradient Richardson number, given by

$$\mathrm{Ri} = \frac{N^2}{S^2}, \tag{3.4}$$

is a local measure of the relative importance of buoyancy and inertia. Here, $N = \sqrt{\alpha g \partial_3 \overline{\Theta}}$ is the Brunt-Väisälä frequency. For stably stratified flows, $N^2 > 0$. $S = \sqrt{2 S_{ij} S_{ij}}$ is the norm of the mean strain-rate tensor.

The gradient Richardson number, as well as its critical value for linear stability, was conjectured by Taylor (1915) and proven by Miles (1961). Howard (1961) generalized the proof, showing that for a critical gradient Richardson number, $\mathrm{Ri}_c > 0.25$, everywhere in a continuously stratified parallel flow in the inviscid limit, linear stability is ensured.

On dimensional grounds, global measures of the Richardson number can be defined, such as the bulk and friction Richardson numbers,

$$\mathrm{Ri}_b = \alpha g L \delta \Theta / U_b^2 \tag{3.5a}$$

$$\mathrm{Ri}_\tau = \alpha g L \delta \Theta / u_\tau^2 \tag{3.5b}$$

respectively. Here, U_b is the bulk velocity. Alternatively, the flux Richardson number, $\mathrm{Ri}_f = G_k / P_k$, which equals the ratio of buoyancy destruction to shear production of turbulence kinetic energy, can be used.

Other nondimensional numbers also exist to quantify the degree of stratification. The Grashof number, $\mathrm{Gr} = \mathrm{Re}^2 \mathrm{Ri}$, is common in natural convection problems, and the internal Froude number, $\mathrm{Fr}' = 1/\sqrt{\mathrm{Ri}_b}$, relates a characteristic flow velocity to a characteristic internal wave velocity.

Paper III compares the implications of common measures of stratification in the case of stably stratified, turbulent channel flow.

Chapter 4

The atmospheric boundary layer

The atmospheric boundary layer (ABL) is a region of continuous turbulence close to the surface of the earth. It is bounded by a sharp top region which instantaneously can have a width of similar order as the Kolmogorov length scale. The thickness of the ABL itself varies greatly, from tens of meters to a few kilometers. Generally, stable boundary layers, such as the nocturnal ABL or the ABL in polar areas, are shallower than their unstable counterparts, so-called *convective* boundary layers.

The study of the ABL is complicated by its extreme Reynolds numbers ($\mathrm{Re} \gtrsim 10^8$), the enormous variation in conditions (both spatially and temporally) and the interplay between rotation, buoyancy, and turbulence. Long averaging times are required to obtain converged statistics – the turnover time for the larger eddies can be up to an hour or more – resulting in much scatter in the available data from field measurement campaigns (cf. e.g. Wyngaard and Coté, 1971; Caughey et al., 1979; Lenschow et al., 1980; Banta, 1985; Högström, 1988; Lemone et al., 1999; Mahrt and Vickers, 2002).

The surface layer, which comprises perhaps 10 % of the ABL[1], is the best understood part of the ABL, mainly because more empirical data is available and due to the successful application of Monin-Obhukov similarity theory (Foken, 2006).

Above the ABL, there is a region of stably stratified laminar flow whose wind

[1]Generally, the surface layer denotes the region of approximately constant fluxes, in which the logarithmic velocity profile is also a valid approximation.

velocity is referred to as the *geostrophic wind*. The geostropic wind results from a balance between Coriolis forces, due to the Earth's rotation, and pressure gradients. Under steady, horizontally homogeneous conditions, the mean horizontal momentum conservation equation for the geostrophic wind thus becomes

$$0 = -\frac{1}{\rho}\partial_i P - 2\epsilon_{ijk}\Omega_j U_k, \tag{4.1}$$

in which Ω_j is the rate of rotation of the Earth. The last term in Eq. (4.1) thus represents the cross product of rotation and velocity, i.e. the Coriolis term. From Eq. (4.1) it can also be seen (by scalar multiplication with u_i) that the geostrophic wind velocity is parallel to the isobars.

The geostrophic wind field can be seen as a first approximation to the wind field inside the ABL as well, particularly outside of the tropics. However, in most cases the effects of friction from the Earth's surface and induced turbulent stresses are essential to the flow dynamics.

On average, ABL flow is a balance between Coriolis forces, pressure gradients, and Reynolds stress divergences. However, from an order-of-magnitude analysis, it can be shown that the Coriolis forces can be neglected if

$$U/L \gg \Omega \text{ or } U/L \ll \Omega,$$

since they will not have a significant effect on the scales of the flow in these cases. Here, $\Omega \sim 10^{-4}$ s is the rate of rotation of the Earth, and U and L are characteristic velocity and length scales. A similar well-known criterion is that the Rossby number be small, i.e. $\mathrm{Ro} = U/Lf \ll 1$, where $f = 2\Omega_3$ is the Coriolis parameter.

As an example, for a geographical area of 500 $\times$ 500 m^2 and an assumed wind velocity of 5 ms^{-1}, $U/L \sim 10^{-2}$ and Coriolis forces can thus be assumed negligible. In this case, the system reduces to a Poiseuille-like flow.

The stable ABL is of particular relevance to the present thesis, and it is also the least understood (cf. Section 3). Challenges particularly related to the study of the stable ABL include its strong dependence on topography (Caughey et al., 1979; Snyder, 1985), difficulties related to relaminarization (Fernando, 2003; Flores and Riley, 2011), and causes and effects of low-level jets (Stensrud, 1996). The latter

is a high-altitude peak in wind velocity which surpasses the geostrophic wind velocity and changes direction during the diurnal cycle.

The ABL typically becomes stable at night (the so-called *nocturnal boundary layer*) and during the winter season in polar areas. Stably stratified conditions may also occur locally due to dispersion of gases denser than the surrounding air.

4.1 Internal gravity waves

Internal gravity waves, i.e. waves caused by density gradients in a fluid, are naturally occurring in most stably stratified flows, cf. e.g. Papers II–IV. In the presence of velocity shear, such waves become susceptible to Kelvin-Helmholtz (KH) instabilities, causing the waves to grow into what is often called KH *billows*, shown in Figure 4.1 (top), which break and generate turbulence.

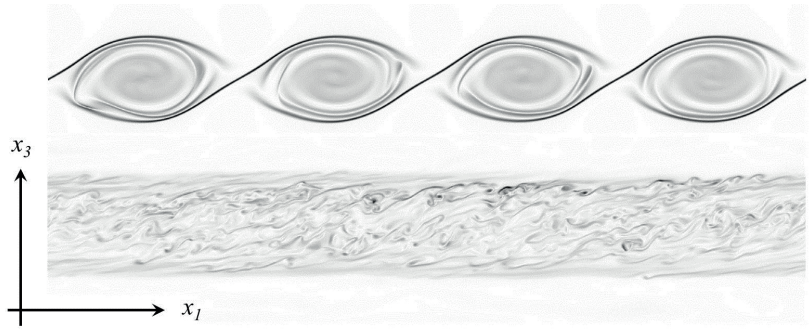

Figure 4.1: KH billows from a DNS simulation (cf. Papers I and II), visualized by enstrophy. Top: Flow shortly after formation of billows. Bottom: Flow a long time after wave breaking. Figure adapted from Paper II.

Expressed in terms of a streamfunction, the so-called Taylor-Goldstein equation governs the dynamics of KH instabilities (i.e. flow perturbations) in a continuously stratified, inviscid, parallel flow. From the Taylor-Goldstein equation, it can be shown (Howard, 1961) that a necessary – but not sufficient – condition for

the instability of internal gravity waves is

$$\mathrm{Ri}_g < \frac{1}{4},$$

cf. Section 3.3.

KH billows are a rather common feature of stably stratified geophysical flows, both in the ocean and in the atmosphere (Smyth and Moum, 2012). In the latter case, the billows are sometimes "visualized" by clouds, as exemplified in Figure 4.2. KH instabilities have also been produced experimentally, cf. e.g. Thorpe (1987); De Silva et al. (1996).

Figure 4.2: KH billows in the atmosphere, visualized by cloud formations over Mount Duval, Australia. Photo courtesy of *Wikipedia*.

KH billows are of particular interest to the present thesis since they, at a later stage, lead to a prolonged state of stably stratified, nearly horizontally homogeneous turbulence, shown in Figure 4.1 (bottom), before the turbulence ultimately decays, and the flow relaminarizes. Such a state is thus a naturally occuring case of stably stratified free-shear flow. The full temporal evolution of KH billows is discussed more thoroughly in e.g.Fritts et al. (1996); Palmer et al. (1996); Werne et al. (2005); Thorpe (2012); Smyth and Moum (2012).

The analyses of Papers I and II are based on the horizontally homogeneous

stage of the KH evolution, but the evolution of the instabilities up to this point is not studied in the present thesis.

4.2 Numerical simulations of the ABL

Since field measurements of atmospheric flows are so demanding, numerical simulations have become increasingly popular as a means to investigate the dynamics of the ABL. As already alluded to (Section 2.5), LES was developed to answer the demands for improved simulations in the field of meteorology.

Deardorff (1970) was the first to apply the LES methodology with subgrid modeling, and subsequent simulations, e.g. by Moeng (1986); Nieuwstadt and De Valk (1987); Mason and Derbyshire (1990), have in large part used largely similar codes. The latter simulation was also among the first LES studies of the stably stratified ABL.

These simulations, as well as more recent work on both stable ABLs (Kosovic and Curry, 2000; Beare et al., 2006) and convective ABLs (Patton et al., 2003; Wang et al., 2007), are generally in good agreement with both field data and reliable similarity models.

Due to the enormous Reynolds numbers in the atmosphere, DNS cannot be used to simulate the ABL. Nevertheless, DNS studies have been used increasingly more often in recent years as a means to investigate specific mechanisms of the ABL in a more "prototypical" flow configuration. The open-channel simulations of e.g. Nieuwstadt (2005); Flores and Riley (2011) constitute idealized approximations to the stable ABL, and Garg (1996); García-Villalba and del Alamo (2011) have performed closed-channel simulations from similar motivations.

In the present thesis, the main focus is on the interaction between stable stratification and mean shear, motivated by its relation to medium-range (ten to a few hundred meters) dispersion. Coriolis forces have therefore been excluded from all numerical simulations, and the wind velocity is aligned with the mean pressure gradient. A recent example of a simulation in which both rotation and buoyancy affect the resulting flow can be found e.g. in the stratified Ekman layer simulation of Deusebio et al. (2014).

Presently, Papers I and II are treatments of numerical data from a Kelvin-Helmholtz instability (see Section 4.1), an instability which occurs only in stably

stratified flows. In Papers III and IV, plane channel flow (see Section 5) with varying levels of stable stratification has been simulated, as an approximation to the surface layer of a stable ABL.

Chapter 5

Fully-developed channel flow

Channel flow constitutes a case highly suitable for numerical simulations; it is easily defined and characterized, it is statistically steady and homogenous in two directions while still maintaining anisotropic, inhomogeneous turbulence, and it is relatively easy to design equivalent experimental trials. As already mentioned (Section 4.2), channel flow is also a rather common approximation to ABL flow.

Fully-developed channel flow is defined as a flow between two infinite, parallel plates. The flow may be driven by a volume force, such as a mean pressure gradient (Poiseuille flow) or a Coriolis term, or motion can be generated via boundary conditions, e.g. by moving one of the plates (Couette flow).

5.1 Poiseuille flow

The geometry of the channel is shown in Figure 5.1. Defining a control volume as sketched in the figure, it is also clear that a force balance in the x-direction yields

$$\begin{aligned} 2Hp_0 - 2H(p_0 + \mathrm{d}\tilde{p}) - 2\tau_w \mathrm{d}x &= 0 \\ -\frac{\mathrm{d}\tilde{p}}{\mathrm{d}x} &= \frac{\tau_w}{H}, \end{aligned}$$

in which $\tau_w = \mu \partial_3 U|_{\text{wall}}$ is the wall shear stress. The force balance must of course hold for both laminar and turbulent flow.

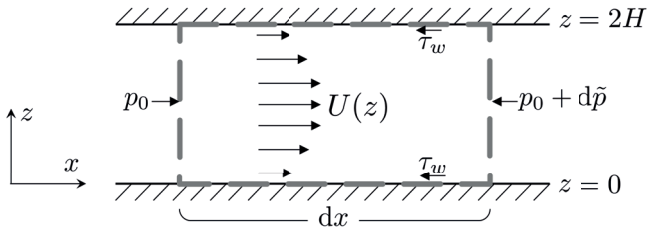

Figure 5.1: Schematic illustration of closed-channel flow. The dashed grey-colored rectangle represents a control volume.

By dimensional arguments, it is common to define a friction velocity, u_τ, via

$$\rho u_\tau^2 \equiv \tau_w.$$

In the case of wall-bounded flows, the friction Reynolds number is often defined as

$$\mathrm{Re}_\tau = \frac{u_\tau H}{\nu}.$$

The friction Reynolds number fully characterizes the flow, provided no other volume forces (e.g. buoyancy or rotation) are present. The force balance can be expressed in terms of the friction Reynolds number,

$$-\frac{\mathrm{d}\tilde{p}}{\mathrm{d}x} = \frac{\mu^2 \mathrm{Re}_\tau^2}{\rho H^3}. \tag{5.1}$$

In simulations of turbulent channel flow with a specified Reynolds number Re_τ, it is thus common to drive the flow by imposing a volume force equal to the pressure gradient required to satisfy Eq. (5.1).

The first DNS of fully-developed channel flow was performed by Kim et al. (1987) for a channel of $\mathrm{Re}_\tau = 180$. Due to the low Reynolds number of the simulation, the logarithmic region was very short, and no inertial subrange could be discerned. Later simulations (Moser et al., 1999) used the same numerical code to produce data for $Re_\tau = 395$ and $Re_\tau = 590$, and this database is still used extensively by turbulence modelers for verification purposes. More recently, channel

simulations of significantly higher Reynolds numbers have appeared, such as that by Hoyas and Jiménez (2006) with $\mathrm{Re}_\tau = 2,003$. Such high-Reynolds number simulations may shed light on new scaling laws as well as possible laws of universality of turbulent flows (Smits et al., 2011).

5.1.1 Wall variables

In the context of wall-bounded flows, so-called *wall variables* or *viscous units* are often used. These are non-dimensional scales, and the viscous length and mean-velocity scales are defined, respectively, as

$$z^+ = \frac{z u_\tau}{\nu} \qquad U^+ = \frac{U}{u_\tau}.$$

Note particularly that $z^+ = 1$ corresponds to $z = \eta$, i.e. one viscous unit corresponds to the smallest turbulent length scale of the flow (the Kolmogorov scale).

Turbulent wall-bounded flows are typically divided into several layers, as summarized in Figure 5.2. The *viscous layer*, $z^+ \lesssim 30$, is highly affected by viscosity and relatively insensitive to flow details far from the wall. The viscous layer can be divided into the *linear sublayer*, $z^+ \lesssim 5$, in which $U^+ \sim z^+$, and the *buffer sublayer*, $5 \lesssim z^+ \lesssim 30$.

Further from the wall, but still within what is referred to as the *inner region*, the *logarithmic layer*, $30 \lesssim z^+ \lesssim 300$, is located. From dimensional arguments, it can be shown that $\partial_3 U \sim u_\tau / z$ in this region. The von Kármán constant, κ_K, is typically taken as the constant of proportionality, so that, expressed in viscous units,

$$\frac{\mathrm{d}U^+}{\mathrm{d}z^+} = \frac{1}{\kappa_\mathrm{K} z^+},$$

which can be integrated to yield the well-known *law of the wall*,

$$U^+(z^+) = \frac{1}{\kappa_\mathrm{K}} \ln(z^+) + C,$$

where C is a constant.

The law of the wall holds for $z \ll H$. In the *outer region*, $z/H \gtrsim 0.4$, the law of the wake applies (cf. e.g. Pope, 2000, p. 305).

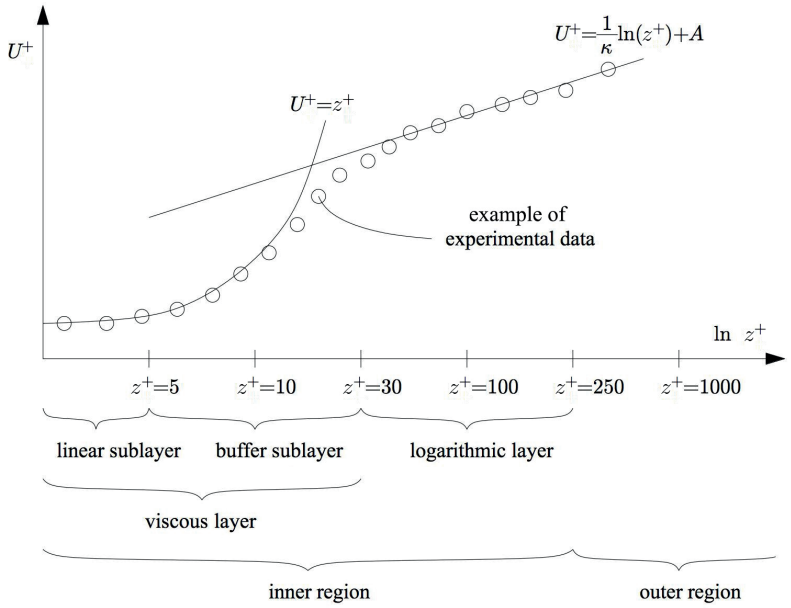

Figure 5.2: Schematic illustration of the layers in wall-bounded turbulent flow.

It is easily shown that for flow, characterized by friction Reynolds number Re_τ, in a channel of half-width H,

$$z^+ = \frac{z}{H}\mathrm{Re}_\tau,$$

from which it can be seen that if $\mathrm{Re}_\tau \lesssim 100$, no logarithmic layer will be discernible.

5.2 Stratified channel flow

As already implied, channel flow constitutes a highly suitable starting point for studying effects of stratification on boundary-layer turbulence.

The first experimental work on stratified channel flow appears to have been reported by Britter (1974), although the study by Arya (1975) of an open-channel flow might be better known. Since then, numerous other experimental measurements (cf. e.g. Fukui et al., 1983; Komori et al., 1983; Morel et al., 1991; Ohya and Uchida, 2003), mostly in open channels, have been complemented by a growing database of computational results:

The first DNS of weakly stratified channel flow was performed by Garg (1996), but the first DNS of a uniformly sheared and linearly stratified free flow was conducted more than two decades ago (Gerz et al., 1989). Prior to the simulation by Garg (1996), LES results from stable atmospheric boundary-layer simulations were also published (cf. e.g. Mason and Derbyshire, 1990; Coleman et al., 1992), as discussed in Section 4.2.

After Garg (1996), a number of authors have published results from numerical simulations of stratified channel flow (cf. e.g. Garg et al. (2000); Iida et al. (2002); Moestam and Davidson (2005) or references in the following paragraph), documenting reduced vertical mixing, increased mean centerline velocities, reduced friction coefficients and Nusselt numbers, thermoclinic temperature profiles, and internal gravity waves, among others.

More recently, García-Villalba and del Alamo (2011) investigated the apparent disagreement between results of Garg et al. (2000) and Iida et al. (2002), and those of Armenio and Sarkar (2002). The first two papers reported simulations that produced laminar flows at significantly lower friction Richardson number ($\mathrm{Ri}_\tau = 45$) than the latter. Armenio and Sarkar (2002) maintained turbulent flow up to $\mathrm{Ri}_\tau = 480$, the highest Richardson number simulated at the time, which is much closer to the theoretically predicted value of Gage and Reid (1968). García-Villalba and del Alamo (2011) found that a likely reason for premature relaminarization in the cases of Garg et al. (2000) and Iida et al. (2002) could be artificial constraints due to too small computational domains, which is also consistent with one of the main conclusions of Moestam and Davidson (2005). Apart from this important conclusion, the data of García-Villalba and del Alamo (2011) agreed well with findings from earlier research on stratified channel flow.

In the present thesis, as is typical in stratified channel flow simulations, the stratification is achieved by "heating" the top wall and "cooling" the bottom wall, i.e. by prescribing different Dirichlet boundary conditions for the temperature

field. Alternatively, Neumann boundary conditions can be used, in which different heat fluxes are imposed at the two walls. In stratified channel flow, the Reynolds number alone is not enough to fully characterize the flow. The Prandtl number,

$$\mathrm{Pr} = \frac{\nu}{\gamma},$$

quantifies the ratio of momentum to thermal diffusivity, ν and γ (cf. Section 3.2), respectively. In air, $\mathrm{Pr} \approx 0.7$, but in fluids of higher Prandtl numbers, it is worth noting that the laminar thermal boundary layer can be significantly smaller than the momentum boundary layer, since (White, 2006, p. 328)

$$\delta_\theta \sim \frac{\delta_u}{\mathrm{Pr}^{0.4}},$$

where δ_u and δ_θ are the boundary layer thicknesses of the momentum and thermal layers, respectively. This has potential implications for the near-wall resolutions in DNS and LES flows.

The relative effect of buoyancy to shear can be expressed by different quantifies (cf. Paper III), but the friction Richardson number, defined in Eq. (3.5b), is a common global characterization of stratified, wall-bounded, turbulent flows.

Armenio and Sarkar (2002) utilize the linear analysis of Gage and Reid (1968) to show that laminar Poiseulle flow with $\mathrm{Re}_\tau = 180$ is linearly stable for $\mathrm{Ri}_\tau > 881$. This critical value also seems reasonable from their simulations and the subsequent simulations of García-Villalba and del Alamo (2011). A similar analysis implies that the flow simulated in Papers III and IV, with $\mathrm{Re}_\tau = 395$, would be linearly stable for $\mathrm{Ri}_\tau \gtrsim 9 \cdot 10^3$.

It seems evident that recent research is consistent on most key aspects of channel flow under the imposition of stable stratification. A large part of the current research challenges appears to be related to achieving data from higher Reynolds-number and Richardson-number flows. Paper III and IV of the present thesis use finely resolved LES data to quantify and discuss the changes in dynamics and turbulence structures associated with stable stratification, a topic generally lacking in previously published research.

5.3 Aerosol transport

A scalar governed by the advection-diffusion equation given in Eq. (2.3) can be defined as *passive* if it does not affect the evolution of the velocity field, i.e. if there are no source terms in Eq. (2.1) which depends on the advected scalar. Temperature is usually considered an *active* rather than passive scalar, since it affects momentum conservation through the buoyancy term.

Transport and dispersion of passive scalars are governed by turbulence and mean flow advection, rather than by molecular diffusion. Passive contaminant transport is therefore expected to depend strongly on the kinematic structure of the flow field.

The release of passive scalars in a turbulent boundary layer simulation is of high practical relevance. In engineering flows, chemical mixing processes and species transport in pipes constitute common examples. In the ABL, particularly in the surface layer, contaminants from industrial sites, pollutants from city centers, chemicals from explosives, and smoke from artillery grenades all constitute transport processes that in many cases can be approximated as passive scalars.

The case study of Fossum et al. (2012), in which aerosol dispersion from an industrial plant was investigated, exemplifies the application of aerosol transport computations. In the study, passive scalar transport (as well as Lagrangian particle tracking) was simulated in combination with large-eddy simulation of the wind field. The concentration field in the near-surface layer was in excellent agreement with measurements from wind-tunnel experiments.

It should be noted that some aerosols are not governed by Eq. (2.3), i.e. they do not behave simply as tracer particles. Due to size, shape, or density, the weight and drag of the aerosols may cause their *particle relaxation time*, τ_p, to be significantly higher than the typical time scale of the flow, τ_f. For approximately spherical particles, the relaxation time is given by

$$\tau_p = \frac{d_p^2 \rho_p}{18\mu},$$

where d_p and ρ_p are the diameter and density of the particle, respectively. The

flow time scale can be estimated from the mean strain rate, i.e.

$$\tau_f = \frac{1}{\sqrt{2\tilde{S}_{ij}\tilde{S}_{ij}}}.$$

The ratio between the particle and flow time scales is given by the Stokes number,

$$\mathrm{St} = \frac{\tau_p}{\tau_f},$$

and if this ratio becomes large, the aerosols do not simply obey the advection-diffusion equation.

Instead, a Lagrangian approach is usually employed, in which each particle is tracked individually. The motion of a particle is governed by the balance of forces acting on the particle, cf. e.g. Maxey and Riley (1983), which can be integrated forward in time to calculate the particle's path. While physically accurate, the Lagrangian framework suffers from the need of a high number of particles to reach statistical convergence, requiring much more computational resources than simply solving Eq. (2.3).

Aerosols can generally be treated as passive scalars if $\mathrm{St} \ll 1$, and if the particle concentration is "dilute", i.e. when the volume fraction of aerosols is $\lesssim 10^{-6}$ (Elgobashi, 1994).

Most studies of passive scalar transport in channel flows, such as Kim and Moin (1989); Kawamura et al. (1998); Abe et al. (2004), have considered only neutral flows. Additionally, they have usually not investigated releases from point or line sources. Rather, volumetric source terms or particular scalar boundary conditions have been used to specify scalar sources. Bakosi et al. (2007) modeled scalar transport from sources at two different heights in an isothermal channel by means of probability density functions, and scalar transport in shear-free, stratified flow was investigated experimentally and numerically by Nagata and Komori (2001). Lagrangian particle dispersion in the stably stratified regime has been studied by e.g. Kimura and Herring (1996); Dong and Chen (2011).

While previously reported simulations can shed light on important aspects of the dispersion, many real-life contaminant releases, such as smoke from a pipe, gas from a nozzle, or aerosols from an industrial plant, resemble point or line sources of passive scalars, such as those used in the unstably stratified open-

channel simulations of Liu and Leung (2006) or the experimental and numerical studies of isothermal channel flow by Lavertu and Mydlarski (2005); Germaine et al. (2014).

Passive scalar transport is an important topic of Paper III, and conclusions from Paper II and IV also have implications for scalar transport processes.

Chapter 6

Computational fluid dynamics

As discussed in Section 2, the governing equations of fluid motion cannot generally be solved analytically. The solution of Eqs. (2.1)-(2.2), as well as possible additional equations, by means of numerical algorithms on a computer is commonly called *computational fluid dynamics* (CFD). Numerical modeling is not the topic of the present thesis, but since numerical methods are an inevitable part of any turbulent flow simulation, the most relevant points are discussed in the following.

The methodology of CFD varies greatly from application to application and software to software, but the general workflow is often as outlined in Figure 6.1. The main steps in the workflow will be described briefly.

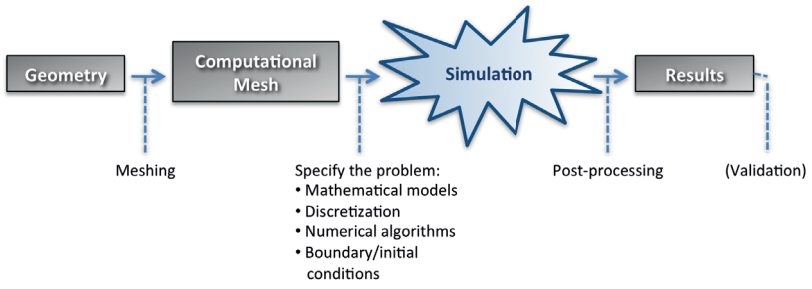

Figure 6.1: Typical CFD workflow (from left to right).

6.1 Geometry and meshing

Firstly, the geometry of the problem needs to be supplied, whether this be a simple box with periodic boundaries or a complex urban area with lots of details. In the case of complex geometries, it is often necessary to clean up the geometry to reduce the demands for computational resources when solving the governing equations numerically. For example, details with relatively little impact on the flow field, such as window-frames or road signs in the case of an urban city center, can and should be removed.

With the rare exception of certain spectral solvers, the geometry and the volume it encloses must be subdivided into computational *cells* for the CFD solver to give reasonable results. This is a process referred to as *meshing* or *gridding*. Depending on the application, everything from a few thousand to hundreds of millions of cells may constitute a computational mesh.

Usually, the mesh is not uniformly spaced; regions of high shear, for example, tend to require much smaller cells to capture the large velocity field gradients. In stratified simulations, the smallest eddies affected by buoyancy, characterized by the Ozmidov scale,

$$\ell_O = \sqrt{\frac{\varepsilon}{N^3}},$$

where $\varepsilon = \varepsilon_{ii}/2$ is the turbulence kinetic energy dissipation rate, should be resolved for reliable simulation results. Furthermore, the mesh must adhere to the shape of the geometry while retaining adequate quality; particularly, large cell aspect ratios, highly acute or obtuse angles between cell edges, and rapidly varying cell sizes should be avoided.

In a DNS or LES without wall modeling, the smallest scales of motion need to be resolved near solid surfaces if wall-generated shear is the main instigator of turbulence. This means that the computational cells need to be of a size comparable to the Kolmogorov scale, η (cf. Section 2.3). The criterion that the wall-variable z^+ should be close to unity in the wall-adjacent computational cells is commonly used in wall-bounded flow simulations. Exact requirements for mesh resolution at the wall do not exist, but most authors agree with e.g. Choi and Moin (2012) that in terms of wall variables, the wall-adjacent cells should be of dimensions $(\Delta x^+, \Delta y^+, \Delta z^+) \sim (100, 20, 1)$ or smaller.

6.2 Numerical discretization

The equations that are solved in a CFD program come in numerous variants. In the case of DNS, Eqs. (2.1)-(2.2) or equivalent equations, such as vorticity-streamfunction formulations, are used – see e.g. Gresho (1991) for a comprehensive list of possible formulations. In LES, Eqs. (2.16)-(2.17) or equivalent equations are implemented.

The equation set needs to be approximated and discretized so it can be solved numerically. The three most common methods for approximating and discretizing the equations are the finite element, spectral, and finite difference methods. The latter also includes the finite-volume method (FVM), which will be discussed in the following.

For FVM solvers, the discretization entails recasting the governing equations in conservative form so that each computational cell in the mesh can be treated as a discrete control volume. The solver can thus calculate the solution to the transport equations by considering the fluxes through the surfaces of each cell in the computational mesh. As an example, consider the advection term of Eq. (2.1). Integrating over a volume and using Gauss' divergence theorem, the term can be rewritten

$$\iiint_V u_k \partial_k u_i \,\mathrm{d}V = \iint_S u_k u_i n_i \,\mathrm{d}S$$

where V and S are the volume and surface of a control volume – typically a compuational cell – respectively.

The resulting integral system can be discretized, i.e. converted into a system of algebraic equations, by employing a number of substitutions, which depend on the specific variety of FVM used, for the terms in the integrated equations. For incompressible flows, the discretized equations are then solved for each computational cell in the mesh simultaneously, time step by time step. The solution for a given time step is computed by producing a linear system of equations of rank $N_{\mathrm{tot}} \times N_{\mathrm{tot}}$, where N_{tot} is the total number of computational cells, which is solved iteratively.

The quality of a numerical solver is often judged in terms of its convergence, consistence, and stability (Versteeg and Malalasekera, 1995, p. 6), but in practice versatility and ease-of-use might be equally important. FVM solvers generally perform well in most of these areas, although finite element and spectral methods

typically have higher convergence rates. The latter may be important if higher order statistics is essential to the data analysis.

In the context of LES, the numerical algorithm is particularly relevant since the mesh can be quite coarse compared to DNS meshes. The truncation of data due to the discrete mesh acts as an implicit filtering operation. Consequently, the terms *subfilter* and *subgrid* are often used interchangeably. In reality, a distinction can be made between subfilter stresses, which are stresses modulated by an explicit filter, and subgrid stresses, which are stresses removed due to numerical truncation. In practice, FVM-LES codes perform both these operations simultaneously; the mesh *is* essentially the filter.

Carati et al. (2001) show that for a wide class of explicit LES filters, such as the Gaussian filter, the limit of infinite numerical resolution implies that no information is actually lost when the filter is applied; the full flow fields can be reconstructed as long as all (infinitely many) wave modes are retained. The effect of a finite computational mesh is essentially to remove higher-order wavenumbers, thus truncating the solution and making the filter irreversible. In other words, it is the numerical discretization which removes information.

One important practical implication is that the LES-RSTE will never balance perfectly on a finite computational mesh, since the combined filtering and discretization operation irreversibly removes information from the solution. This information cannot be perfectly modeled by the subgrid terms[1].

Conservation of kinetic energy is also of particular importance to LES solvers; dissipative numerical schemes tend to overwhelm the effect of the subgrid (and molecular) viscosity, whereas straight-forward, non-dissipative central-differencing schemes lead to numerical instability (Mahesh et al., 2004). Hence, the use of robust, non-dissipative numerical algorithms is crucial to the success of an LES solver.

6.2.1 CDP – a multipurpose LES code

Papers III and IV are based on simulations performed with the FVM-based solver CDP v3.5.1 (Mahesh et al., 2002; Ham and Iaccarino, 2004; Mahesh et al., 2004;

[1]The same is true for any other LES transport equation involving subgrid terms, except when the variables are explicitly conserved by the numerical algorithm.

Ham et al., 2006), and the most important features of the solver will be summarized in the following.

The incompressible version of the solver, `Cliff`, stores all flow fields in the mesh nodes. The code is second-order in space and up to second-order in time, using a Crank-Nicholson/Adams-Bashforth time-stepping algorithm. The pressure-coupling is based on a fractional-step approach.

The calculation of the subgrid viscosity in CDP's dynamic Smagorinsky model is described in Section 2.5.1. CDP uses a test filter with twice the size of the ordinary filter width.

The advantages of CDP are similar to those of other FMV-based methods mentioned earlier; in particular, the code uses unstructured meshes to be able to handle complex geometries, and it is relatively easy to extend the code by programming additional boundary conditions, source terms or data-processing algorithms. Additionally, the numerical algorithms in CDP are formulated so as to maximize conservation of kinetic energy without loss of numerical stability. Recent versions of the code is written in C++ and is highly parallelized.

The major drawback is reduced accuracy compared to e.g. finite element methods applied on similar computational meshes.

Chapter 7

Summary of results

The main results, as well as a short description, of each individual paper in the present thesis are listed in Section 7.1. The main results of the thesis as a whole can be categorized by the three objectives in Section 1.1 and are as follows:

Establish a methodology which enables the simulation of stably stratified, turbulent boundary-layer flows in a flexible solver which can easily be extended to more complex problems.

The parallelized energy-conserving FVM solver CDP is highly suitable for LES. The incompressible version of the code, `Cliff`, is very robust and can handle unstructured meshes of great complexity.

In the present work, `Cliff` has been extended to be able to handle stratification via the Boussinesq approximation with temperature as an active scalar. The results from several stably stratified simulations are consistent and agree very well with previously reported DNS and LES results in the literature. Unstable stratification should work similarly well, but has not yet been verified. The Boussinesq implementation can be used with arbitrary geometries and in conjunction with other volume forces, such as Coriolis forces, thus constituting an important step towards the ability to simulate stratified ABLs with `Cliff`.

Additionally, the calculation of budget terms of the RSTE, the turbulence kinetic energy transport equation, and the scalar variance transport equation have been implemented in `Cliff`, also with satisfactory results. These higher-order statistics converge well with increasing computational mesh resolution and show

agreement with expected results. An exception is the dissipation rate, which is often under-predicted due to its high sensitivity to mesh resolution. Structure tensors (Kassinos et al., 2001) have also been computed in `Cliff`, with good results.

Investigate how the imposition of stable stratification affects turbulent shear flow, with particular emphasis on the turbulence dynamics and structures.

In channel flow, the present work suggests that three distinct regions of the channel can be defined for each (symmetric) half-height from the wall. The *shear region* ($z/H \lesssim 0.2$) is virtually unaffected by stable stratification for all the levels of Ri_τ investigated. In the *transition region* ($0.2 \lesssim z/H \lesssim 0.8$), the shear is dynamically most important, but the turbulence is modified by the presence of buoyancy. The *buoyancy region* ($z/H \gtrsim 0.8$) is dominated by buoyancy, meaning that there is local destruction of turbulence, that turbulence is significantly altered due to stratification, and that internal waves become increasingly dominant.

From the literature, it is clear that the most obvious effects of imposed stable stratification are reduced vertical turbulent fluctuations and transport, as well as a related increase in anisotropy. The results of the present work also reveal important changes in the structural state of turbulence. The "compression" of the vertical structure of turbulence can be quantified by the dimensionality tensor and is significant (up to 50 % in channel flow with $\mathrm{Ri}_\tau = 240$). Additionally, the transition region in wall-bounded flow is strongly homogenized by increased stratification, which suggests an increased decoupling between the shear region and buoyancy region.

From the free-shear flow data, it appears that the Reynolds stress anisotropy increase up to a certain level of stratification, corresponding to $\mathrm{Ri}_g \approx 0.4$. However, for stronger stratification the anisotropy begins to decrease, most likely caused by relaminarization.

The dynamics of the turbulence is affected very differently by stratification in wall-bounded flow and free-shear flow. In the former, both P_k and ε increase. The buoyancy destruction term is generally small, but in the buoyancy region there is net destruction of energy, since $P_k + G_k - \varepsilon < 0$ there. The increased anisotropy of the Reynolds stresses also causes increased inter-componental energy transfer, quantified by increasing values of ϕ_{ij}.

In the case of free-shear flow, the most notable find related to turbulence dynamics is the exchange of roles of shear production and buoyancy destruction. Contrary to the "regular" case, such as channel flow, the shear production term actually removes energy from the turbulent field near the edge of the shear layer, whereas the buoyancy destruction term is an instigator of turbulence. It is shown that this is related to the observed turbulent flux reversal, i.e. a change in sign of $\langle uw \rangle$. It is also found that, for the Reynolds numbers considered presently, the viscous dissipation rate is highly anisotropic.

Another interesting feature of free-shear flow is how the imposition of strong stable stratification seems to mimic the non-local pressure effects of an impenetrable wall. However, it is found that the kinematic blocking effect of walls is not emulated by the imposed stable stratification. Turbulence models employed in stably stratified flows ought to include non-local information to incorporate important effects of stratification. Since the dimensionality tensor resembles its near-wall behavior, models based on this non-local single-point quantity might be beneficial.

Examine the effects of stable stratification on scalar dispersion in a turbulent boundary layer.

Transport and dispersion of any passive contaminant are governed by turbulence and mean flow advection, rather than by molecular diffusion. Passive contaminant transport is therefore expected to respond significantly to changes in the kinematic structure of the flow field caused by the imposition of a stably stratified background.

As an example, the changes in Reynolds stress anisotropy under imposed stratification has consequences for dispersion modeling; Gaussian dispersion models commonly utilize the velocity variance to estimate the deformation of contaminant clouds, cf. e.g. Sykes and Gabruk (1996). The variance is thus important for estimating the spread of a Gaussian puff as well as the decay of peak concentration.

The distinct differences between the components of the Reynolds stress and dimensionality tensors, as well as their respective responses to imposed stratification, have implications for both momentum and scalar transport. As an example,

under homogeneous turbulence, Eq. (2.14) implies that

$$\langle u_i u_j \rangle = q^2 \delta_{ij} - D_{ij} - F_{ij}.$$

Since the production terms of both momentum and scalar fluxes depend on the Reynolds stresses, it is clear that they can also be written in terms of the dimensionality and circulicity tensors, thereby incorporating variations in turbulence structure. Moreover, non-local effects can be incorporated into eddy-viscosity and eddy-diffusivity models by utilizing dimensionality and circulicity information, such as in the *eddy-axis*-based model of e.g. Kassinos et al. (2006).

In channel flow, the present work shows that passive scalar transport is altered significantly by stable stratification, and the effect of stratification is stronger for scalar releases closer to the buoyancy region. Vertical scalar flux is reduced, leading to inhibited vertical dispersion and higher peak concentrations downstream than in the neutral case. For example, four boundary-layer lengths downstream, peak concentration was more than 50 % higher for $\mathrm{Ri}_\tau = 240$ compared to neutral flow. From the mean scalar concentration transport equation, it is shown that the vertical scalar flux is vital to the evolution of mean concentration.

Whereas peak mean concentration downstream decays exponentially in the neutral case, this is not found to be the case under imposed stratification. Eddy-diffusivity models for scalar transport based on the turbulent Schmidt number ought to take stratification into account to have predictive value.

7.1 Summary of papers

A model for the viscous dissipation rate in stably stratified, sheared turbulence (Paper I)

Kolmogorov's theory postulates that at high Reynolds numbers, turbulent flows exhibit local isotropy. In recent decades, however, increasing amounts of evidence of the contrary has accumulated. In the presence of strong local anisotropy, the isotropic formulation of the viscous dissipation rate, commonly used to estimate the dissipation rate in experimental measurements, becomes inaccurate at best.

In Paper I, a new model for the turbulence dissipation rate in stably stratified

shear turbulence is developed and validated. The functional dependence of the model is derived from first principles and it represents a conceptually new approach in that it depends on the mean temperature field rather than the fluctuating velocity field. This novel feature makes the proposed model a viable candidate for dissipation rate estimates in real-life flows.

Direct numerical simulation data are used to assess the model, and it is shown that the model performs very well, particularly in cases in which the stratification is dynamically dominant.

Additionally, a generalized expression for the so-called mixing coefficient, which is used to predict small-scale mixing processes in the atmosphere, is derived from first principles under the assumption of locally isotropic, incompressible flow.

Anisotropy and shear-layer edge dynamics of statistically unsteady, stratified, sheared turbulence (Paper II)

Direct numerical simulation data of an evolving Kelvin-Helmholtz instability have been analyzed in order to characterize the dynamic and kinematic response of a shear-generated turbulent flow to imposed stable stratification. Anisotropy and shear-layer edge dynamics in the net kinetic energy decay phase of the Kelvin-Helmholtz evolution was the main focus of the study. The energy decay phase is a period of horizontally homogeneous turbulence, which simplifies the analysis greatly.

Results indicate that the flow is locally anisotropic, i.e. even the small scales are anisotropic. Furthermore, the small-scale anisotropy seems to increase at a higher rate than the large-scale anisotropy. The anisotropy of thermal dissipation differs significantly from that of viscous dissipation.

It is found that the Reynolds stress anisotropy increases up to a stratification level roughly corresponding to $\mathrm{Ri}_g \approx 0.4$, but subsequently decreases for higher levels of stratification, most likely due to relaminarization.

The structure tensor framework of Kassinos et al. (2001) is used to quantify the large-scale coherent structures of the turbulence. These structures are cylindrical in the center of the shear layer, whereas they become ellipsoidal in the strongly stratified edge-layer region. The structures of the Reynolds stresses are highly

jetal in the center and become two-componental as stratification increases. Stratification affects all scales, but it seems to affect larger scales to a higher degree than smaller scales and thermal scales more strongly than momentum scales.

The strong stable stratification at the edge of the shear layer is highly reminiscent of the non-local pressure effects of solid walls. However, the kinematic blocking inherently associated with impermeable walls is not observed in the edge layer.

Vertical momentum flux reversal is found in part of the shear layer. The roles of shear and buoyant production of turbulence kinetic energy are exchanged, and shear production is transferring energy into the mean flow field, which may lead to relaminarization. The change in dynamics near the edge of the shear layer has important implications for predictive turbulence model formulations.

Numerical simulation of stably stratified channel flow. Part I: Characterization, dynamics, and scalar transport (Paper III)

This paper is based on high-resolution large-eddy simulations performed with the finite-volume method research code, CDP (cf. Section 6.2.1).

The effect of increasingly stable stratification ($\mathrm{Ri}_\tau = \{0, 20, 60, 120, 240\}$) on fully developed, turbulent channel flow at $\mathrm{Re}_\tau = 395$ has been assessed. Changes in mean flow quantities as well as velocity and temperature fluctuations are discussed. The level of stratification has been characterized by several Richardson numbers, the Froude number, and the buoyancy Reynolds number, among others. The energy budgets for the Reynolds stresses, the turbulence kinetic energy, and the temperature fluctuations have been analyzed.

It is found that stable stratification increases mean velocities in the channel, and the turbulence intensity decays. Vertical turbulent fluxes of momentum and temperature are reduced, and the Reynolds stress anisotropy is altered, particularly close to the channel centerline. There is evidence of increased decoupling between the near-wall region and the center region of the channel with increased stratification, related to homogenization of the intermediate region.

Three distinct regions of the channel can be defined, depending on the strength of the buoyancy.

The turbulence kinetic energy budget is relatively unchanged under imposed stratification, but net destruction of turbulence kinetic energy in the core of the channel occurs due to increased viscous dissipation and buoyancy destruction. The temperature fluctuation budget is more affected than the kinetic energy budget.

Passive scalars have been released at different heights in the channel, and the effect of stratification on their evolutions downstream have been quantified. The transport is significantly altered by stable stratification; vertical dispersion is strongly inhibited, and peak mean concentrations downstream remain much higher than in the neutral case, in which the concentration follows exponential decay.

Numerical simulation of stably stratified channel flow. Part II: Turbulence structures (Paper IV)

This paper is based on the same simulations as Paper III, but the present paper considers the effects of stratification on the structural state of the turbulence.

The response of commonly used length-scale measures are quantified and given a physical interpretation. One-point structure tensors carrying non-local information are utilized to assess the changes in turbulence structure under imposed stratification. Specifically, the inhomogeneity, dimensionality, and circulicity tensors are investigated and discussed, with particular emphasis on physical implications. The structure tensors are also briefly compared to more traditional two-point measures such as integral length scales and energy spectra. Finally, the changes in both kinematic and spatial turbulence anisotropy are examined.

It is found that imposed stable stratification reduces almost all relevant turbulence length scales as well as amplifies the anisotropy of both the Reynolds stresses and the coherent flow structures. The latter also undergoes a change in its axisymmetrical state. The effects of buoyancy are much more significant in the region with weak shear far from the channel walls, and on the larger scales of motion. Near-wall streaks remain unaffected, whereas in the core region of the channel, internal gravity waves emerge. The homogenization of the intermediate region between the viscous/buffer layer and the core of the channel is quantified by the inhomogeneity tensor. Almost everywhere, vertical motion is inhibited by stratification, and the coherent structures are compressed in the vertical direction.

Bibliography

Abe, H., Kawamura, H., and Matsuo, Y. Surface heat-flux fluctuations in a turbulent channel flow up to Re_τ = 1020 with Pr = 0.025 and 0.71. *International Journal of Heat and Fluid Flow*, 25 (3):404–419, 2004.

Armenio, V. and Sarkar, S. An investigation of stably stratified turbulent channel flow using large-eddy simulation. *Journal of Fluid Mechanics*, 459:1–42, 2002.

Arya, S. Buoyancy effects in a horizontal flat-plate boundary layer. *Journal of Fluid Mechanics*, 68 (02):321–343, 1975.

Bakosi, J., Franzese, P., and Boybeyi, Z. Probability density function modeling of scalar mixing from concentrated sources in turbulent channel flow. *Physics of Fluids*, 19 (11):115106, 2007.

Banta, R. M. Late-morning jump in TKE in the mixed layer over a mountain basin. *Journal of the Atmospheric Sciences*, 42 (4):407–411, 1985.

Beare, R. J., Macvean, M. K., Holtslag, A. A., Cuxart, J., Esau, I., Golaz, J.-C., Jimenez, M. A., Khairoutdinov, M., Kosovic, B., Lewellen, D., et al. An intercomparison of large-eddy simulations of the stable boundary layer. *Boundary-Layer Meteorology*, 118 (2):247–272, 2006.

Bendat, J. S. and Piersol, A. G. *Engineering Applications of Correlation and Spectral Analysis* (Wiley-Interscience, New York, 1980).

Bhattacharya, A., Kassinos, S. C., and Moser, R. D. Representing anisotropy of two-point second-order turbulence velocity correlations using structure tensors. *Physics of Fluids*, 20:101502, 2008.

Boussinesq, J. *Théorie analytique de la chaleur: mise en harmonie avec la thermodynamique et avec la théorie mécanique de la lumière*, vol. 2 (Gauthier-Villars, 1903).

Britter, R. *An Experiment on Turbulence in a Density-Stratified Fluid*. Ph.D. thesis, Monash University, 1974.

Carati, D., Winckelmans, G. S., and Jeanmart, H. On the modelling of the subgrid-scale and filtered-scale stress tensors in large-eddy simulation. *Journal of Fluid Mechanics*, 441 (1):119–138, 2001.

Caughey, S., Wyngaard, J., and Kaimal, J. Turbulence in the evolving stable boundary layer. *Journal of the Atmospheric Sciences*, 36 (6):1041–1052, 1979.

Charney, J. G., Fjörtoft, R., and Neumann, J. v. Numerical integration of the barotropic vorticity equation. *Tellus*, 2 (4):237–254, 1950.

Choi, H. and Moin, P. Grid-point requirements for large eddy simulation: Chapman's estimates revisited. *Physics of Fluids*, 24:011702, 2012.

Coleman, G., Ferziger, J., and Spalart, P. Direct simulation of the stably stratified turbulent ekman layer. *Journal of Fluid Mechanics*, 244:677–712, 1992.

De Silva, I., Fernando, H., Eaton, F., and Hebert, D. Evolution of Kelvin-Helmholtz billows in nature and laboratory. *Earth and Planetary Science Letters*, 143 (1):217–231, 1996.

Deardorff, J. Preliminary results from numerical integrations of the unstable planetary boundary layer. *Journal of the Atmospheric Sciences*, 27:1209–1211, 1970.

Deusebio, E., Brethouwer, G., Schlatter, P., and Lindborg, E. A numerical study of the unstratified and stratified Ekman layer. *Journal of Fluid Mechanics*, 755:672–704, 2014.

Dong, Y. and Chen, L.-F. The effect of stable stratification and thermophoresis on fine particle deposition in a bounded turbulent flow. *International Journal of Heat and Mass Transfer*, 54:1168–1178, 2011.

Durbin, P. A. and Petterson Reif, B. A. *Statistical Theory and Modeling for Turbulent Flows, Second Ed.* (John Wiley & Sons Ltd, West Sussex, England, 2011).

Elgobashi, S. On predicting particle-laden turbulent flows. *Appl. Sci. Res.*, 52:309–329, 1994.

Fernando, H. Turbulent patches in a stratified shear flow. *Physics of Fluids*, 15 (10):3164–3169, 2003.

Feynman, R. P., Leighton, R. B., and Sands, M. The Feynman Lectures on Physics, Mainly Mechanics, Radiation, and Heat, Volume I. 1963.

Flores, O. and Riley, J. Analysis of turbulence collapse in the stably stratified surface layer using direct numerical simulation. *Boundary-Layer Meteorology*, 139:241–259, 2011.

Foken, T. 50 years of the Monin–Obukhov similarity theory. *Boundary-Layer Meteorology*, 119 (3):431–447, 2006.

Fossum, H., Reif, B., Tutkun, M., and Gjesdal, T. On the use of computational fluid dynamics to investigate aerosol dispersion in an industrial environment: A case study. *Boundary-Layer Meteorology*, 144:21–40, 2012.

Fritts, D. C., Palmer, T. L., Andreassen, Ø., and Lie, I. Evolution and breakdown of Kelvin-Helmholtz billows in stratified compressible flows. Part I: Comparison of two-and three-dimensional flows. *Journal of the Atmospheric Sciences*, 53 (22):3173–3191, 1996.

Fukui, K., Nakajima, M., and Ueda, H. A laboratory experiment on momentum and heat transfer in the stratified surface layer. *Quarterly Journal of the Royal Meteorological Society*, 109 (461):661–676, 1983.

Gage, K. and Reid, W. The stability of thermally stratified plane Poiseuille flow. *Journal of Fluid Mechanics*, 33 (01):21–32, 1968.

García-Villalba, M. and del Alamo, J. Turbulence modification by stable stratification in channel flow. *Physics of Fluids*, 23:045104, 2011.

Garg, R., Ferziger, J., Monismith, S., and Koseff, J. Stably stratified turbulent channel flows. I. Stratification regimes and turbulence suppression mechanism. *Physics of Fluids*, 12:2569, 2000.

Garg, R. P. *Physics and modeling of stratified turbulent channel flows*. Ph.D. thesis, Stanford University, 1996.

Germaine, E., Mydlarski, L., and Cortelezzi, L. Evolution of the scalar dissipation rate downstream of a concentrated line source in turbulent channel flow. *Journal of Fluid Mechanics*, 749:227–274, 2014.

Germano, M., Piomelli, U., Moin, P., and Cabot, W. A dynamic subgrid-scale eddy viscosity model. *Physics of Fluids A: Fluid Dynamics*, 3:1760, 1991.

Gerz, T., Schumann, U., and Elghobashi, S. Direct numerical simulation of stratified homogeneous turbulent shear flows. *Journal of Fluid Mechanics*, 200 (1):563–594, 1989.

Grant, H., Stewart, R., and Moilliet, A. Turbulence spectra from a tidal channel. *Journal of Fluid Mechanics*, 12 (02):241–268, 1962.

Gresho, P. M. Incompressible fluid dynamics: Some fundamental formulation issues. *Annual Review of Fluid Mechanics*, 23 (1):413–453, 1991.

Ham, F. and Iaccarino, G. Energy conservation in collocated discretization schemes on unstructured meshes. *Annual Research Briefs*, 2004:3–14, 2004.

Ham, F., Mattsson, K., and Iaccarino, G. Accurate and stable finite volume operators for unstructured flow solvers. Tech. rep., Center for Turbulence Research, 2006.

Helgeland, A., Andreassen, Ø. ., Ommundsen, A., Reif, B. A. P., Werne, J., and Gaarder, T. Visualization of the energy-containing turbulent scales. *IEEE*, 2005.

Högström, U. Non-dimensional wind and temperature profiles in the atmospheric surface layer: A re-evaluation. In *Topics in Micrometeorology. A Festschrift for Arch Dyer*, pp. 55–78 (Springer, 1988).

Howard, L. N. Note on a paper of John W. Miles. *J. Fluid Mech*, 10 (4):509–512, 1961.

Hoyas, S. and Jiménez, J. Scaling of the velocity fluctuations in turbulent channels up to Re = 2003. *Physics of Fluids*, 18:011702, 2006.

Hunt, J. C., Wray, A., and Moin, P. Eddies, streams, and convergence zones in turbulent flows. Tech. rep., Center for Turbulence Research, 1988.

Iida, O., Kasagi, N., and Nagano, Y. Direct numerical simulation of turbulent channel flow under stable density stratification. *International Journal of Heat and Mass Transfer*, 45 (8):1693–1703, 2002.

Jeong, J. and Hussain, F. On the identification of a vortex. *Journal of Fluid Mechanics*, 285:69–94, 1995.

Kassinos, S., Langer, C., Kalitzin, G., and Iaccarino, G. A simplified structure-based model using standard turbulence scale equations: Computation of rotating wall-bounded flows. *International Journal of Heat and Fluid Flow*, 27 (4):653–660, 2006.

Kassinos, S., Reynolds, W., and Rogers, M. One-point turbulence structure tensors. *Journal of Fluid Mechanics*, 428:213–248, 2001.

Kassinos, S. C., Langer, C. A., Haire, S. L., and Reynolds, W. C. Structure-based turbulence modeling for wall-bounded flows. *International Journal of Heat and Fluid flow*, 21 (5):599–605, 2000.

Kassinos, S. C. and Reynolds, W. C. *A structure-based model for the rapid distortion of homogeneous turbulence*. Ph.D. thesis, to the Department of Mechanical Engineering.Stanford University, 1995.

Kawamura, H., Ohsaka, K., Abe, H., and Yamamoto, K. DNS of turbulent heat transfer in channel flow with low to medium-high Prandtl number fluid. *International Journal of Heat and Fluid Flow*, 19 (5):482–491, 1998.

Keating, A., Piomelli, U., Balaras, E., and Kaltenbach, H.-J. A priori and a posteriori tests of inflow conditions for large-eddy simulation. *Physics of Fluids*, 16:4696, 2004.

Kim, J. and Moin, P. Transport of passive scalars in a turbulent channel flow. In *Turbulent Shear Flows 6*, pp. 85–96 (Springer, 1989).

Kim, J., Moin, P., and Moser, R. Turbulence statistics in fully developed channel flow at low Reynolds number. *Journal of Fluid Mechanics*, 177 (1):133–166, 1987.

Kimura, Y. and Herring, J. Diffusion in stably stratified turbulence. *Journal of Fluid Mechanics*, 328:253–269, 1996.

Kline, S. and Robinson, S. Quasi-coherent structures in the turbulent boundary layer. I – Status report on a community-wide summary of the data. *Near-Wall Turbulence*, 1:200–217, 1990.

Kolmogorov, A. N. Dissipation of energy in locally isotropic turbulence. In *Dokl. Akad. Nauk SSSR*, vol. 32, pp. 16–18 (1941a).

Kolmogorov, A. N. The local structure of turbulence in incompressible viscous fluid for very large Reynolds numbers. In *Dokl. Akad. Nauk SSSR*, vol. 30, pp. 299–303 (1941b).

Komori, S., Ueda, H., Ogino, F., and Mizushina, T. Turbulence structure in stably stratified open-channel flow. *Journal of Fluid Mechanics*, 130:13–26, 1983.

Kosovic, B. and Curry, J. A. A large eddy simulation study of a quasi-steady, stably stratified atmospheric boundary layer. *Journal of the Atmospheric Sciences*, 57 (8):1052–1068, 2000.

Kundu, P. K. and Cohen, I. M. *Fluid Mechanics, Fourth Ed.* (Academic Press, USA, 2008).

Lavertu, R. and Mydlarski, L. Scalar mixing from a concentrated source in turbulent channel flow. *Journal of Fluid Mechanics*, 528:135–172, 2005.

Lemone, M. A., Zhou, M., Moeng, C.-H., Lenschow, D. H., Miller, L. J., and Grossman, R. L. An observational study of wind profiles in the baroclinic convective mixed layer. *Boundary-Layer Meteorology*, 90 (1):47–82, 1999.

Lenschow, D., Wyngaard, J. C., and Pennell, W. T. Mean-field and second-moment budgets in a baroclinic, convective boundary layer. *Journal of the Atmospheric Sciences*, 37 (6):1313–1326, 1980.

Lesieur, M. *Large-eddy simulations of turbulence* (Cambridge University Press, 2005).

Lilly, D. K. The representation of small scale turbulence in numerical simulation experiments. In *Proceedings of the IBM Scientific Computing Symposium on Environmental Sciences*, vol. Form no. 320-1951, pp. 195–210 (IBM, 1967).

Lilly, D. K. A proposed modification of the Germano subgrid-scale closure method. *Physics of Fluids A: Fluid Dynamics*, 4 (3):633–635, 1992.

Liu, C. and Leung, D. Turbulent transport of passive scalar behind line sources in an unstably stratified open channel flow. *International Journal of Heat and Mass Transfer*, 49 (23-24):4305–4324, 2006.

Lumley, J. L. and Newman, G. R. The return to isotropy of homogeneous turbulence. *Journal of Fluid Mechanics*, 82 (1):161–178, 1977.

Mahesh, K., Constantinescu, G., Apte, S., Iaccarino, G., Ham, F., and Moin, P. Progress toward large-eddy simulation of turbulent reacting and non-reacting flows in complex geometries. *Annual Research Briefs*, pp. 115–142, 2002.

Mahesh, K., Constantinescu, G., and Moin, P. A numerical method for large-eddy simulation in complex geometries. *Journal of Computational Physics*, 197:215–240, 2004.

Mahrt, L. Stably stratified atmospheric boundary layers. *Annu. Rev. Fluid Mech.*, 46 (3):23–45, 2014.

Mahrt, L. and Vickers, D. Contrasting vertical structures of nocturnal boundary layers. *Boundary-Layer Meteorology*, 105 (2):351–363, 2002.

Mason, P. and Derbyshire, S. Large-eddy simulation of the stably-stratified atmospheric boundary layer. *Boundary-Layer Meteorology*, 53 (1-2):117–162, 1990.

Maxey, M. R. and Riley, J. J. Equation of motion for a small rigid sphere in a nonuniform flow. *Physics of Fluids*, 26 (4):883–889, 1983.

McLoughlin, T., Laramee, R. S., Peikert, R., Post, F. H., and Chen, M. Over Two Decades of Integration-Based, Geometric Flow Visualization. *Computer Graphics Forum*, 29 (6):1807–1829, 2010.

Miles, J. W. On the stability of heterogeneous shear flows. *J. Fluid Mech*, 10 (4):496–508, 1961.

Moeng, C.-H. Large-eddy simulation of a stratus-topped boundary layer. Part I: Structure and budgets. *Journal of the Atmospheric Sciences*, 43 (23):2886–2900, 1986.

Moestam, R. and Davidson, L. Numerical simulations of a thermocline in a pressure-driven flow between two infinite horizontal plates. *Physics of Fluids*, 17 (7):075109, 2005.

Morel, R., Alcaraz, E., Ayrault, M., Zegadi, R., and Mejean, P. Effects of thermal stable stratification on turbulent boundary layer characteristics. *Atmospheric Environment. Part A. General Topics*, 25 (7):1263–1269, 1991.

Moser, R., Kim, J., and Mansour, N. Direct numerical simulation of turbulent channel flow up to $\mathrm{Re}_\tau = 590$. *Physics of Fluids*, 11:943, 1999.

Nagata, K. and Komori, S. The difference in turbulent diffusion between active and passive scalars in stable thermal stratification. *Journal of Fluid Mechanics*, 430:361–380, 2001.

Nieuwstadt, F. T. M. Direct numerical simulation of stable channel flow at large stability. *Boundary-Layer Meteorology*, 116 (2):277–299, 2005.

Nieuwstadt, F. T. M. and De Valk, J. P. J. M. M. A large eddy simulation of buoyant and non-buoyant plume dispersion in the atmospheric boundary layer. *Atmospheric Environment*, 21 (12):2573–2587, 1987.

Ohya, Y. and Uchida, T. Turbulence structure of stable boundary layers with a near-linear temperature profile. *Boundary-Layer Meteorology*, 108 (1):19–38, 2003.

Palmer, T. L., Fritts, D. C., and Andreassen, Ø. Evolution and breakdown of Kelvin-Helmholtz billows in stratified compressible flows. Part II: Instability structure, evolution, and energetics. *Journal of the Atmospheric Sciences*, 53 (22):3192–3212, 1996.

Panton, R. L. Overview of the self-sustaining mechanisms of wall turbulence. *Progress in Aerospace Sciences*, 37 (4):341–383, 2001.

Patton, E., Sullivan, P., and Davis, K. The influence of a forest canopy on top-down and bottom-up diffusion in the planetary boundary layer. *Quarterly Journal of the Royal Meteorological Society*, 129 (590):1415–1434, 2003.

Pecnik, R., Kassinos, S., Duraisamy, K., and Iaccarino, G. Towards an Accurate and Robust Algebraic Structure Based Model. In *Proceedings of the Summer Program*, p. 283 (2012).

Phillips, N. A. The general circulation of the atmosphere: A numerical experiment. *Quarterly Journal of the Royal Meteorological Society*, 82 (352):123–164, 1956.

Pope, S. B. *Turbulent Flows* (Cambridge University Press, Cambridge, United Kingdom, 2000).

Reif, B. and Andreassen, Ø. On local isotropy in stratified homogeneous turbulence. *SIAM Journal on Applied Mathematics*, 64:309–321, 2003.

Reif, B., Werne, J., Andreassen, Ø., Meyer, C., and Davis-Mansour, M. Entrainment-zone restratification and flow structures in stratified shear turbulence. *Studying Turbulence Using Numerical Simulation Databases-IX*, pp. 245–256, 2002.

Reynolds, O. An experimental investigation of the circumstances which determine whether the motion of water shall be direct or sinuous, and of the law of resistance in parallel channels. *Proceedings of the Royal Society of London*, 35 (224-226):84–99, 1883.

Reynolds, O. On the dynamical theory of incompressible viscous fluids and the determination of the criterion. *Proceedings of the Royal Society of London*, 56 (336-339):40–45, 1894.

Robinson, S. K. Coherent motions in the turbulent boundary layer. *Annual Review of Fluid Mechanics*, 23 (1):601–639, 1991.

Saddoughi, S. G. and Veeravalli, S. V. Local isotropy in turbulent boundary layers at high reynolds number. *Journal of Fluid Mechanics*, 268:333–372, 1994.

Sagaut, P. *Large Eddy Simulation for Incompressible Flows: An Introduction*. Scientific Computation (Springer, 2006), 3rd ed. ISBN 9783540263449. URL `http://books.google.no/books?id=ODYiH6RNyoQC`.

Smagorinsky, J. General circulation experiments with the primitive equations: I. The basic experiment. *Monthly Weather Review*, 91 (3):99–164, 1963.

Smits, A. J., McKeon, B. J., and Marusic, I. High-Reynolds number wall turbulence. *Annual Review of Fluid Mechanics*, 43:353–375, 2011.

Smyth, W. and Moum, J. Anisotropy of turbulence in stably stratified mixing layers. *Physics of Fluids*, 12:1343, 2000.

Smyth, W. D. and Moum, J. N. Ocean mixing by Kelvin-Helmholtz instability. *Oceanography*, 25 (2):140–149, 2012.

Snyder, W. H. Fluid modeling of pollutant transport and diffusion in stably stratified flows over complex terrain. *Annual Review of Fluid Mechanics*, 17 (1):239–266, 1985.

Stensrud, D. J. Importance of low-level jets to climate: A review. *Journal of Climate*, 9 (8):1698–1711, 1996.

Sykes, R. I. and Gabruk, R. S. A second-order closure model for the effect of averaging time on turbulent plume dispersion. *J. Appl. Meteorol.*, 36:1033–1045, 1996.

Taylor, G. I. Eddy motion in the atmosphere. *Philosophical Transactions of the Royal Society of London. Series A, Containing Papers of a Mathematical or Physical Character*, pp. 1–26, 1915.

Tennekes, H. and Lumley, J. L. *A First Course in Turbulence* (MIT press, 1972).

Thoroddsen, S. and Van Atta, C. The influence of stable stratification on small-scale anisotropy and dissipation in turbulence. *Journal of Geophysical Research*, 97 (C3):3647–3658, 1992.

Thorpe, S. Transitional phenomena and the development of turbulence in stratified fluids: A review. *Journal of Geophysical Research: Oceans (1978–2012)*, 92 (C5):5231–5248, 1987.

Thorpe, S. On the Kelvin–Helmholtz route to turbulence. *Journal of Fluid Mechanics*, 708 (1):1–4, 2012.

Versteeg, H. K. and Malalasekera, W. *An Introduction to Computational Fluid Dynamics: The Finite Volume Method* (Pearson Education, 1995).

Wang, W., Davis, K. J., Yi, C., Patton, E. G., Butler, M. P., Ricciuto, D. M., and Bakwin, P. S. A note on the top-down and bottom-up gradient functions over a forested site. *Boundary-Layer Meteorology*, 124 (2):305–314, 2007.

Werne, J., Lund, T., and Fritts, D. CAP Phase II simulations for the Air Force HEL-JTO project: Atmospheric turbulence simulations on NAVO's 3000-processor IBM P4+ and ARL's 2000-processor Intel Xeon EM64T cluster. In *Users Group Conference, 2005*, pp. 100–111 (IEEE, 2005).

White, F. M. *Viscous Fluid Flow, Third Ed.* (The McGraw-Hill Companies, New York, USA, 2006).

Wyngaard, J. *Turbulence in the Atmosphere* (Cambridge Univ Pr, 2010).

Wyngaard, J. and Coté, O. The budgets of turbulent kinetic energy and temperature variance in the atmospheric surface layer. *Journal of the Atmospheric Sciences*, 28 (2):190–201, 1971.